NTNU – Trondheim
Norwegian University of
Science and Technology

Ship track estimation from single hydrophone data

Magnus Larsen

Electronics System Design and Innovation
Submission date: June 2014
Supervisor: Hefeng Dong, IET
Co-supervisor: Dag Tollefsen, FFI (Forsvarets Forskningsinstitutt)

Norwegian University of Science and Technology
Department of Electronics and Telecommunications

Task Description

The problem is "Ship track estimation from single hydrophone data" and thesis shall develop and test a model-based method for the estimation of the track of a ship from its radiated acoustic noise recorded on a sensor unit (hydrophone) placed on the seabed. A simple and efficient model that describes the spatial structure of the acoustic field at short ranges shall be implemented. A ranging-and-tracking algorithm for a moving ship based on matching of modeled and measured amplitude data shall be implemented and applied to selected data from measurements with the NILUS platform.

Abstract

Passive acoustic range estimation and source tracking using hydrophones have been a problem because of the complexity of the underwater channel. This thesis is concerned with a fast method for the estimation of ship velocity and horizontal range to a surface going vessel using acoustic data from a single hydrophone. The problem is of interest in applications for monitoring of noise from commercial shipping and ship traffic. There has been many who have developed different method for similar problems and this thesis is based on a matched field inversion method.

This method used the analytic Lloyd mirror propagation model which assumes constant sound speed, homogeneous horizontal layers and a single bottom layer, which has reduces accuracy at larger range (300 meter), but is simple and fast. The cost function for matching the recorded data and the modeled data was a modified Bartlett function which calculates the deviation between the ratio of the two data sets and was sensitive to variation in the signal. To reduce the variance in the recorded signal the welch spectral estimation was used. The ASHS and ASDE was implemented for a more efficient search through the parameter space, but a 2D search through the velocity and range parameters was also made to study the uncertainty of the estimations and the effect the different parameters had on the cost function loss. The results of the estimation was compared with the recorded AIS data of the unknown parameters.

The results in this thesis indicate that a close estimation of the ship velocity and horizontal range was possible with the 2D search when presented with a signal with good SNR, reduced variance, low range, good estimation of the source depth, low search interval and a sufficient amount of data which can be used in the estimation. Which also makes it possible to use these parameters for ship tracking. An observation which where made was that the source depth changed the outcome of the estimation drastically. Close estimation with the global search algorithms required higher SNR and knowledge of the unknown parameters that could reduce the search interval.

Sammendrag

Passiv akustisk avstands estimering og kildesporing ved hjelp av hydrofoner har vært et problem på grunn av kompleksiteten i undervannskanalen. Denne avhandlingen er opptatt av en rask metode for estimering av skips hastighet og horisontal avstand til skip ved hjelp av akustiske data fra en enkelt hydrofon. Problemet er av interesse for anvendelser innen overvåking av støy fra kommersiell skipsfart og skipstrafikk. Det har vært mange som har utviklet andre metode for lignende problemer, og denne oppgaven er basert på en matchet felt inversjon metode.

Denne metoden anvender den analytiske Lloyd mirror propagasjons modellen som forutsetter konstant lydhastighet, homogene horisontale lag, og et enkelt bunnsjikt, som har redusert nøyaktighet ved større avstander (300 meter), men er en enkel og rask modell. Kost funksjonen for å sammenliknet de målte dataene og de modelerte dataene var en modifisert Bartlett funksjon som beregner forskjellen mellom forholdet i de to datasettene, og var naturligvis følsomme for variasjoner i signalet. For å redusere variasjonen i det målte signalet så ble en welch spektral estimering brukt. ASHS og ASDE har blitt implementert for et mer effektivt søke igjennom parameter rommet, men et 2D søk igjennom hastighet og avstands parameterene ble også gjort for åstudere usikkerheten i estimatene og hvordan de ulike parametrene påvirket kost funksjons tapet. Resultatene av estimeringene ble sammenlignet med de AIS registrerte dataene av de ukjente parametrene.

Resultatene i denne avhandlingen indikerer at en god estimering av skipets hastighet og den horisontale avstanden var mulig med et 2D søk når metoden ble gitt med et signal med god SNR, redusert varians, kort avstands parameter, god estimering av kildedybde og tilstrekkelig mengde data som kan brukes i estimeringen. En observasjon som ble gjort var at kilde dybden endrer resultatet av estimeringen drastisk og ble da brukt som en tredje ukjent parameter i de globale søkealgoritmene. Godt estimering med de globale søkealgoritmene krevde høyere SNR og kunnskap om de ukjente parametrene som kan redusere søkeintervallet.

Preface

This thesis has been written at the Norwegian University of Science and Technology, spring 2014. The work has been carried out at the Department of Electronics and Telecommunications and concludes my Master of Science degree in Electronics.

The assignment was given by Norwegian Defense Research Establishment (FFI), which has provided all the necessary data and information to conduct the research for this thesis.

I would like to thank my supervisor Hefeng Dong for help and guidance with my thesis. I would also thank my co-supervisor Dag Tollefsen at FFI for his guidance and help resolving problems. Lastly I would like to thank my friends and family for their support.

Magnus Larsen
NTNU, Trondheim
June, 2014

Contents

List of Figures

List of Tables

Chapter 1

Introduction

This chapter consists of an introduction to the thesis, with previous work, interest of subject and a structure of the thesis.

1.1 Background

There has been interest in range estimation and ship tracking for various reasons since the creation of the ship. This may be accomplished by using various methods on recorded hydrophone data.

Some bio-acoustician have used a single hydrophone to calculate the depth/range of phonating diving animals, where the standard one-hydrophone localization method uses multi path transmissions of the animal phonations as a substitute for a vertical hydrophone array, [11]. Others are interesting in ship localization using ship noise, [17]. The approach to achieve this was using an array of hydrophones, where the relative arrival times are used as data in an array element localization inversion method to estimate both the hydrophone and ship location based on an iterated linearization of the acoustic ray equations. The Maritime Systems Division has been interesting in passive acoustic tracking, [22]. This method uses covariance matrix of the pseudo-coordinate track representation for tracking. These are just a few who have taken an interest in this kind of estimations, but there is not known to be not many who have explored the problem that is presented.

FFI have provided the problem for this thesis and has developed a demonstrator system for sensor networks underwater, named NILUS (Networked Intelligent Underwater Sensors) from [20]. The battery-powered sensor nodes are released into the water and lands on the ocean floor, where they can detect the passing ships on or in the water, and send this information to the operations center through sub sea network. NILUS was designed to evaluate and demonstrate the potential for sensor networks under water and has been used in several trials and exercises both nationally and internationally. FFI wants to use this system for range estimations and source tracking of ships to monitoring noise from commercial shipping and ship traffic. The NILUS uses passive hydrophones and is equipped with a single hydrophone which can be used for range and ship velocity estimation, see [21].

This thesis is based on the project "Ship range estimation from single hydrophone data", which has been done as preparation to the thesis, started fall 2013, and was delivered 20th of December the same year. Gathering of information on the theory and testing by simulations with synthetic data was done in the project and the method used in the project is the same as in the thesis. The method, which is used in this thesis, is a matched field method used by Wilmut and Chapman, see [18]. One important difference is that their work has been done to estimate range for a source being dragged by a boat, rather using the emitted ship noise in the estimation. The inversion method compares the recorded propagation field with a modeled propagation field and finds the parameters which gives the best match of propagation.

Inversion methods are effective in estimating large number of unknown parameters. Such methods are applied for example in the oil industry, in seismic, where large areas of ocean floor are supposed to be mapped with large arrays of hydrophones. Global search algorithms are usually utilized for optimizing the inversion methods for more efficiency. In this case it's particularly interesting to see how the Lloyd mirror propagation model are handling the problem because of it simplicity.

1.2 Objectives

The main objectives in this thesis are

1. Use signal processing on the recorded data to reduce the variance in the noisy signal and extract the recorded amplitude data at a given frequency

at a given time.

2. Further develop the matched field method from the project, such as make an global search algorithm and expand operating area of the propagation model.

3. Find sufficient estimates of the horizontal range and ship velocity for some of the recorded data sets which FFI has provided for recreating the ship path as tracking.

1.3 Approach

There will be used signal processing tools such as FFT (fast Fourier transformation), PSD (Power Spectral Density) and Welch spectral estimation to process the measured data, such that the amplitude value of the recorded pressure can be extracted. A faster search will be achieved by using the two global search algorithms, ASHS and ASDE, and the propagation model will be modified such that this method can be used for cases where the receiver isn't at the sea floor for further study. Good estimation will be found by choosing appropriate parameters in the search model, signal processing models and propagation model. The parameters are found by studying the recorded data and changing the parameters accordingly with trial and error.

1.4 Structure of the Report

The objective of this thesis is to explore if the method in [18] is adequate for estimation in the presented problem and if sufficient estimations can be achieved by using the Lloyd mirror as the propagation model. The work in this thesis is divided into three parts, a signal processing part for handle the recorded hydrophone data, a matched field inversion part which consists of a propagation model, cost function and a search algorithm and the last part is applying the method for the recorded data.

The report of the thesis is therefor structured in this way:

- Establishing the theory of the signal processing and the matched field inversion method in chapter 2.

- The experimental set up is described and environmental data is given in chapter 3.
- How the method is applied is described in section 4.1.
- The implemented matched field method is tested with synthetic noisy data and its theoretical limitations is found in section 4.4.
- The implemented method is applied on the recorded data in section 4.5 .
- The results are evaluated and discussed in both section 4.5 and chapter 5.

Chapter 2

Theory

In this chapter a introduction will be given to the theory of the different methods used in the matched field inversion method.

2.1 Signal processing

The acoustical noise, which is generated by a traveling ship, is recorded, amplified and converted from analog to discrete data. The information that is interesting in this case is the pattern of the acoustical propagation through time and over frequencies. This information is extracted by Fourier transformation of segments of time and averaged. This section is inspired by Stian Cowards thesis [7], which uses the same methods for processing the discrete data and is a former student at NTNU,.

2.1.1 Fourier Transform

Fourier transformation transform the signal in time domain into frequency domain. This makes it possible to analyze the signal in the frequency domain.

The analog time segment $x(t)$, which is sampled at a rate $F_s = \frac{1}{\Delta t}$, will create the discrete time signal $x(n\Delta t) = x(n)$. The discrete Fourier transform (DFT) of a finite energy signal of length N, can then be defined as

$$X(k) = \frac{1}{N}\sum_{n=0}^{N-1} x(n)exp(-i2\pi nk/N) \quad n,k = 0,...,N-1 \tag{2.1}$$

from Digital Signal Processing [19, p. 456], where

$$k = \frac{f}{\Delta f} \tag{2.2}$$

this is the same as FFT in Matlab, except of $1/N$. Here Δf is the frequency resolution of the frequency bin.

$$\Delta f = \frac{F_s}{N}. \tag{2.3}$$

The length of the signal in seconds is

$$T = \frac{N}{F_s} = \frac{1}{\Delta f}. \tag{2.4}$$

2.1.2 Power Spectral Density

The power spectral density (PSD) is often used when considering the source level, but in this case the amplitude of the signal is the required information. The pwelch function in MATLAB returns the PSD of the welch spectral estimation, which is described in section 2.1.3, and the PSD is studied to calculate the amplitude of the signal and to present the recorded data.

The power spectral density of a random stationary process can be obtained by the Wiener-Khintchine theorem, by computing the Fourier transform of the autocorrelation function see [19, p. 966], that is

$$\Gamma(f) = \int_{-\infty}^{\infty} \gamma(\tau)exp(-i2\pi f\tau)d\tau \tag{2.5}$$

where

$$\gamma(\tau) = E[x^*(t)\cdot x(t+\tau)]. \tag{2.6}$$

For a discrete finite signal with the Fourier transformation in equation 2.1, the PSD can be defined, from [19, p. 969], as

$$PSD(k) = 2\frac{|X(k)|^2}{\Delta f} = \frac{2}{F_s N}|\sum_{n=0}^{N-1} x(n)exp(-i2\pi nk/N)|^2 \quad n,k = 0,1,...,N-1 \tag{2.7}$$

where the Fourier transforms symmetrical frequencies is summed up, hence the factor of 2. The amplitude can be converted by just inverting this process, but keep the absolute value.

2.1.3 Welch spectral estimation

The welch spectral estimation is an method where a window function is applied to the time signal to estimate the PSD.

The function of the window is that the discontinuous and attenuation of the signal at the start and the end is removed, which will reduce spectral leakage. There are large variety of window functions, see [9], and can be chosen to the problem presented. The hanning window, which is used here, is based on the power of the cosine. Compared to an rectangular window, this gives lower side-lobes and wider main lobe. This will say less spectral leakage, but the width of the main-lobe controls the ability to distinguish between two close spectral components, which affects the frequency resolution. Therefor there is a natural trade of between frequency resolution and spectral leakage. When the DFT length has the same length as the signal the effect on the resolution from both the window function and the DFT, limits the resolution to the same amount. The frequency resolution for a hanning window for $T = 1$ in this case is approximate 1.4 Hz, where the main lobe is -3 dB and side-lobe is -31.5 dB. Max amplitude error is discussed in [9], where this error is -3.9 dB for the rectangular window and -1.4 dB for the hanning window.

If the window function is $w(n), n = 0,1,...,N_s - 1$, the incoherent gain (normalization) factor can be defined by

$$G_{INC} = \frac{1}{N_s}\sum_{n=0}^{N_s-1} w(n)^2. \tag{2.8}$$

The welch spectral estimation method is taken from [9] and divides the signal *x(n)* of length M into L different overlapping segments with length N_s,

$$x_j(n) = x(n + jD) \qquad \begin{matrix} n = 0, 1, ..., N_s - 1 \\ j = 0, 1, ..., L - 1 \end{matrix} \tag{2.9}$$

where the $j\,D$ is start of the jth segment. If $D = N_s$, there is no overlap and the welch method is just like the Bartlett's method. If the $D = N_s/2$, the overlap is *50 %*, which is perfect for the hanning window and $L = 2M/N_s - 1$.

The PSD for one segment, *j*, is then

$$PSD_j(k) = 2\frac{|X_{w,j}(k)|^2}{\Delta f G_{INC}} = \frac{2}{F_s N G_{INC}} |\sum_{n=0}^{N-1} x_j(n) exp(-i2\pi nk/N)|^2 \quad n, k = 0, 1, ..., N-1 \tag{2.10}$$

where $X_{w,j}(k)$ represent the Fourier transformation of the segment *j*, with a window function. The average PSD is then

$$PSD(k) = \frac{1}{L}\sum_{j=0}^{L-1} PSD_j(k). \tag{2.11}$$

2.2 Propagation model

There are two propagation models which are used in this thesis: Lloyd mirror model and RAM (Range dependent acoustical model). The RAM is a numerical solution of the parabolic equation method, based on the split-step Padè solution and is the same as in the project. The RAM is only used to be compared with the Lloyd mirror and is further described in appendix A. The Lloyd mirror model has been modified to consider the receiver at other depths than the sea floor and the basis is taken from the project.

Lloyd mirror is a classic optical experiment to produce interference pattern and study both constructive and destructive interference. The model is analytical and assume the ocean have horizontal homogeneous layers, which implies that the propagation paths are straight lines. The system is a shallow water waveguide where the bottom is considered to be an infinite layer, which gives only reflection from the sea surface and the sea floor.

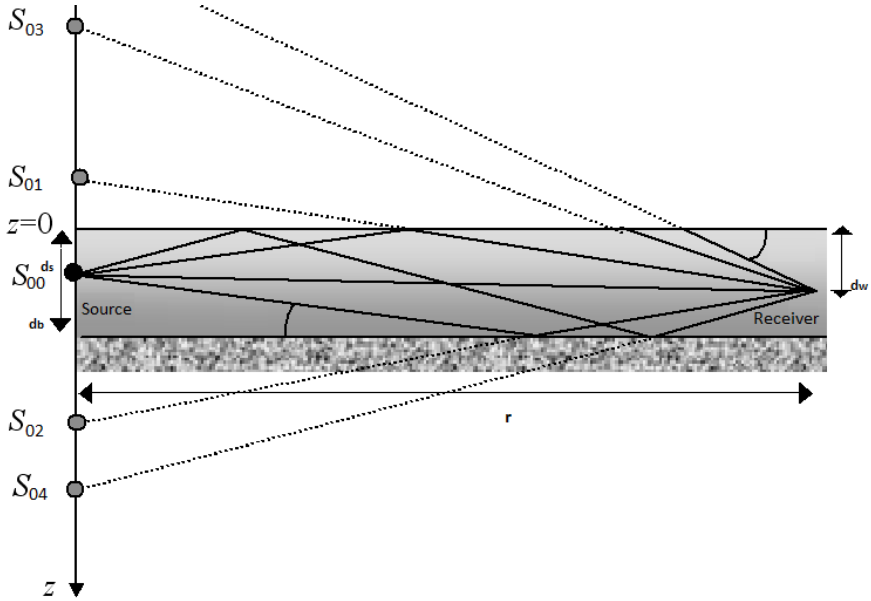

Figure 2.1: The Lloyd mirror paths, taken from [29, p. 34]

In figure 2.1, the water depth is d_b, receiver depth is d_w and source depth is d_s. The source is S_{00} and mirror sources is S_{0X}, where X is number of mirror sources. The field is formulated by the coherent sum of the contributions of the source and its images, where the images are the contribution of the reflections. There will be two sets of images from both the sea surface and sea floor, but in the case where the receiver is located at the sea floor there is only one set of images. This is shown in figure 2.1 where the direct path and the first surface reflected path is a pair. This setup is a multi path field where the components can be organized into pairs in orders, where the two first sets of the images from both the sea surface and sea floor is the first order. To specify, the first order is the contribution of the first four ray paths, the two first rays which hits the surface and the other two are the direct path and the path which is reflected only from the sea floor (the paths of the pair and their reflection from the sea floor). The number of reflections from the sea floor and sea surface increases with the order. For the case where the receiver is at the sea floor the traveling range of the considered path and its reflection are assumed to be equal. The calculated pressure of the direct path and it's reflection at the receiver is given by

$$p_d = \frac{e^{ikR_d}}{R_d} + V\frac{e^{ikR_r}}{R_r} \tag{2.12}$$

where V is the plane-wave reflection coefficient at the sea floor, R_d the distance from the source to the receiver, R_r the distance the reflection paths travels from the source to the receiver and wave number is $k = 2\pi f/c_w$ with f being the frequency of the signal and c_w being the sound speed in water.

$$V = \frac{mcos(\theta_w) - ncos(\theta_s)}{mcos(\theta_w) + ncos(\theta_s)} \tag{2.13}$$

where $m = \rho_s/\rho_w$ and $n = c_w/c_s$, with ρ_s and ρ_w are the density in the sediment and the water, c_s is the sound speed in the sediment and θ_w and θ_s are the incident angle into and out of the sea floor. The reflection coefficient is given in [3, p. 62], this reflection coefficient is used because it is simple and fast to compute.

The components of the field can be separated into down going and up going paths. The Down going paths and its increasing order of bottom reflections are the direct paths and isn't reflected from the sea surface before going downward. The up going paths are the mirror image of the first surface reflection and its increasing order of bottom reflections. This is done by multiplying the field by -1 whenever the the image ray intersects the sea surface images, and by V whenever the image ray intersects the ocean bottom images. The sea surfaces gives a perfect reflection with a 180° phase shift. The slant range of this paths are identified by

$$\begin{aligned}
R_{1-} &= \sqrt{(2nd_b + d_w - d_s)^2 + r^2} \\
R_{2-} &= \sqrt{((2n+1)d_b + d_w - d_s)^2 + r^2} \\
R_{1+} &= \sqrt{(2nd_b + d_w + d_s)^2 + r^2} \\
R_{2+} &= \sqrt{((2n+1)d_b + d_w + d_s)^2 + r^2}
\end{aligned} \tag{2.14}$$

where the $-$ and $+$ are respectively the down going and up going ray paths, r is the horizontal distance between the source and receiver and n is the order of bottom reflection. The slant range can easily be derived by using simple geometry and figure 2.1, assuming straight ray paths. For the case where the receiver is at the sea floor, the slant range is given by $R_- = \sqrt{((2n+1)d_w - d_s)^2 + r^2}$ and $R_+ = \sqrt{((2n+1)d_w + d_s)^2 + r^2}$. The contribution from the down going field is

then given by

$$p_{1-} = \sum_{j=0}^{\infty} (-1)^j (V_{1-})^j \frac{e^{ikR_{1-}}}{R_{1-}}$$
$$p_{2-} = \sum_{j=0}^{\infty} (-1)^j (V_{2-})^{j+1} \frac{e^{ikR_{2-}}}{R_{2-}}, \tag{2.15}$$

and the up going field by

$$p_{1+} = \sum_{j=0}^{\infty} (-1)^{j+1} (V_{1+})^j \frac{e^{ikR_{1+}}}{R_{1+}}$$
$$p_{2+} = \sum_{j=0}^{\infty} (-1)^{j+1} (V_{2+})^{j+1} \frac{e^{ikR_{2+}}}{R_{2+}} \tag{2.16}$$

where j is the order of bottom reflection and V_1-, V_2-, V_1+ and V_2+ are the reflection coefficient from the ocean bottom for the different incident angels derived by the slant range and water depth. The total field is

$$p_t = p_{1-} + p_{2-} + p_{1+} + p_{2+} \tag{2.17}$$

and for practical application for this case the summation in equation 2.15) and (2.16 can be limited to three pairs (third oder of Lloyd mirror), see [18, p. 941].

The Transmission loss can be calculated by comparing the modeled pressure with a reference pressure at 1 meter, like in [12, p. 100],

$$TL = 20log_{10}(\frac{p}{p_{ref}}) \tag{2.18}$$

where the modeled pressure is p and p_{ref} is the reference pressure at 1 meter and is calculated as $p_{ref} = e^{ik}$.

2.3 Cost function

The cost function is the function which matches the recorded data and the modeled data. A cost function (loss function) is a function which maps one or more

variables onto a real number which represents the "cost" of the system. For an optimization problem this value represent the loss and the point is to minimize it. The lower the loss are, the closer to the optimized system it gets.

The [18] propose a cost function and this is the used in this thesis. The multi tone signal is modeled by the Lloyd mirror field model $d_{i,f}(m)$ and is compared with a recorded or synthetic data $d_{i,f}$, where the number of time intervals (time blocks) is given by $i = 1,2,...,n_t$. This time intervals are transformed into the frequency domain and the number of frequency is given by $f = 1,2,...,n_f$. The amplitude data of the Lloyd mirror modeled can be found by taking the absolute value of the calculated pressure. The cost function is given by:

$$E_f(m) = 1 - \frac{\left(\sum_{i=1}^{n_t} \tilde{d}_{i,f}\tilde{d}_{i,f}(m)\right)^2}{\sum_{i=1}^{n_t} \tilde{d}_{i,f}^2 \sum_{i=1}^{n_t} \tilde{d}_{i,f}^2(m)} \tag{2.19}$$

which is the Bartlett mismatch, where $\tilde{d}_{i,f}$ and $\tilde{d}_{i,f}(m)$ are $d_{i,f}$ and $d_{i,f}(m)$ with their time averages subtracted. For data with multiple frequencies, a suitable cost function is given by

$$E(m) = \left[\prod_{f=1}^{n_f} E_f(m)\right]^{1/n_f} \tag{2.20}$$

where the $E_f(m)$ is the misfit at the individual frequency from 2.19 and the $E(m)$ is the overall misfit. The cost function from [18] is derived from [28].

2.4 Search Algorithm

For inversion problems there are usually many unknown parameters and they might vary over large intervals, for effectively finding the best estimation of the parameters a nonlinear global optimization algorithms can be applied. The problem presented only have two parameters that are considered to be unknown, the horizontal range and the ship velocity. This thesis explores three different search algorithms: simple 2D search, ASHS (Adaptiv Simplex Harmonic Search) and ASDE (Adaptiv Simplex Differential Evolution).

The simple 2D search algorithm only work for two parameters and searches through both parameters by applying the cost function on each combination. This makes

a 2D matrix with a value at each combination of the parameters. The simple 2D search algorithm is slow because it has to calculate the cost at each combination of the parameters before a search for the minimum value in this 2D matrix can be made. The global search algorithm is possibly faster with the appropriate control parameters, but the random global search algorithms ASHS and ASDE isn't that simple.

The code of the ASHS and ASDE is take from Niklas S. Skyberg thesis, a former student at NTNU. HS is based on the search for good sounding harmonies when improvising. DE is an evolution based global optimization algorithm, where it takes inspiration of evolution steps to optimized the solution. The ASHS and ASDE algorithms are randomly searching through the parameter space by having a chance of basing the new parameters, which will be explore, on previously explored parameters which gave low loss, or creating an entire new random combination of parameters. This is further description in [23], where the HS and DE are based on [24] and [26].

Chapter 3

Experiment

In this chapter the data set which will be used in the estimation will be described. This includes the equipment, ship recordings, location data and the environment data. The experiment report is called NGAS10 (Next Generation Autonomous System 2010) sea trials and was performed in 2010 by FFI, the information is not open for the public to read, but I have had access to the necessary data for the estimation. The experiment are described in [7] and the data is taken from this thesis, where the data is from the same sea trial.

3.1 Sea trial

The recording system is an easily deployable autonomous underwater sensor network, called NILUS (Network Intelligent Underwater sensor) [21], and have acoustical and magnetic sensors. The NGAS10 sea trial used NILUS nodes and they was deployed several times for recording the ship noise amongst other things. Only one of this node locations is used in this thesis for horizontal range and velocity estimation, the depth and coordinates can be found in table I and can be seen on the map in figure 3.1.

Table I: Depth and coordinates at the four NILUS locations, taken from [7].

NILUS location	Depth (m)	Latitude	Longitude
A	196	59N 28.363	10E 29.142

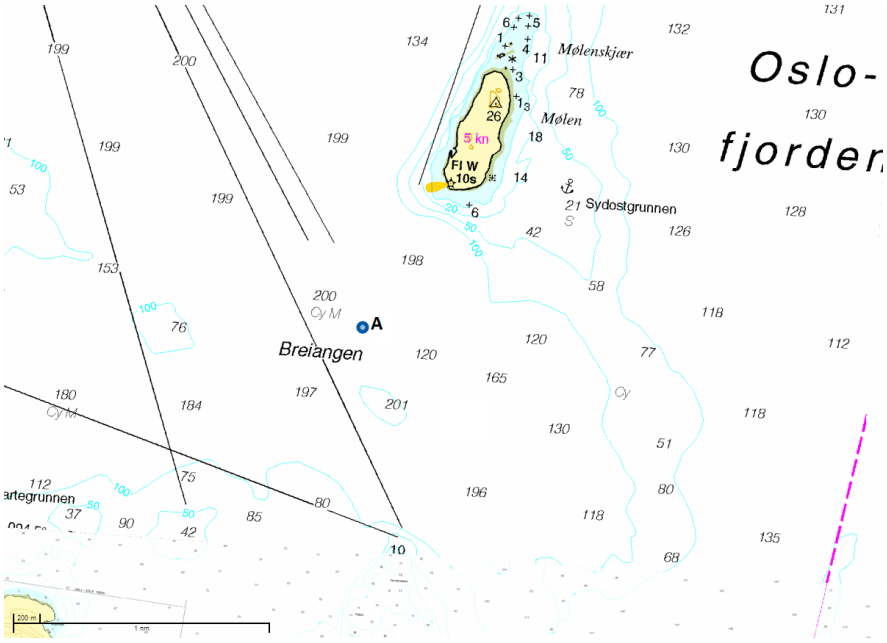

Figure 3.1: The location of the NILUS node locations outside Horten in Breiangen, using the coordinates in table I and a map from Kartverket [15].

3.2 Acoustical Sensors

The NILUS nodes are equipped with two different types of acoustic sensors that are described in [21] and [7], where the DIFAR (Directional Frequency Analysis and Recording) was suitable. This sensor has a known frequency response, where the usable frequency range is from 10 Hz to 3 kHz. The estimation is interested in frequencies between 50 Hz to 1 kHz, which is cowered by this. The factory specification of the passive hydrophone is give in [8]. The acoustical measurement data is recorded on a memory card with sampling frequency of 18 kHz and 24-bit A/D-converter. The recorded data is later decimated to a sampling frequency of 9 kHz and converted into 16-bit a wav-files.

The acoustical modem of the NILUS-node saturated an internal amplifier when it was transmitting and in addition to this problem, there seemed to be some sort of amplitude clipping of the recorded signal at high intensities. The received pressure is normally high at the ships CPA and the recording of the ships passing at a distance shorter than 500-700 meters seemed to experience this clippings.

The maximum deployment depth is a few hundred meters and the accuracy of the displacement is a few meters, this accuracy is dependent on the water speed and the depth. The NILUS node has sensor to measure the depth of the node with an accuracy of ±3 meters of the true depth, see [7], this data is logged and compared with echo-sounders and charts.

3.3 Acoustic data

The GPS information from the AIS data was recorded for the ship passings. To ensure a measurement uninfluenced by other ships, there must be a sufficient time before and after a ship passing where no other ships are in the near vicinity. There is a lot of activity in the fjord and this causes the background noise to be generally high. Smaller vessels as fishing boats and similar, which are not using the AIS system, are operating in the area and might cause unregistered influence on the recording of the ship passing because of higher potential of high SNR. The high background noise and clipping of the amplitude results in low SNR.

There has been given two different recordings of ship passing which has been thought to be suitable for range and velocity estimation. This recordings don't have any or a lot of amplitude clipping in the relevant part of the recording (the recording around the CPA), have relative high SNR such that the propagation pattern is visible and enough time between ship passings. The two ships are Småen and Jumbo and Jumbo is a cargo ship which makes it more likely to be suitable in this thesis. Småen is a smaller vessels and might not be as suitable as Jumbo.

3.4 AIS data

The AIS records data of the ships continuously and for the AIS to give the necessary information the data has been parsed by Høgskolen i Ålesund [13] and processed by FFI. This gives the time and distance to each node located at CPA.

The draft is necessary for calculating the depth of the source, but is unknown for the ship passing as described in [7] and therefor average of the reported drafts of the ship is used in the estimation of the source depth.

The position of the ship is sent at different intervals, see [25], and even fewer might have been recorded by the AIS receiver. Because of this there may occur

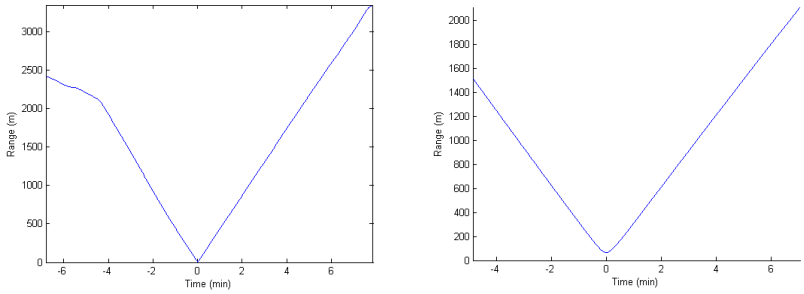

(a) Småen (b) Jumbo

Figure 3.2: The distance between the NILUS-A and the ship using the AIS recording.

error when estimating time and location at the CPA between the NILUS-node and the ship. This are dealt with as described in [7] by interpolating the tracking. The figures 3.2b and 3.2b shows the recorded distance between the NILUS-node and the passing of Småen and Jumbo. The recordings also shows that the ships are traveling with constant ship velocity and in a straight path, except for the first two minutes of the Småen recording.

3.5 Environment data

The wind speed during the 17th and 18th of June had a mean of about 7 m/s, and there was no noticeable rain occurring during the period of the recordings, as described in [7]. This indicates calm weather that should not influence the recording very much, see section 4.1.4 on noise. This suits the propagation model which isn't considering rain or uneven sea surface in the calculation.

A CTD (conductivity, temperature, depth) probe, see [2], was used to take SSP (sound speed profile) measurements at several times and locations during the sea trials. The SSP is shown over depth in figure 3.3, where some were taken at shallow and deep water, they are however very similar at the overlapping depths. This shows that there exist a horizontal homogeneous water column throughout the area and a sound propagation channel at 30-40 meter can be considered to be present during the trial. Change in weather condition might be responsible for the variation in the upper layer.

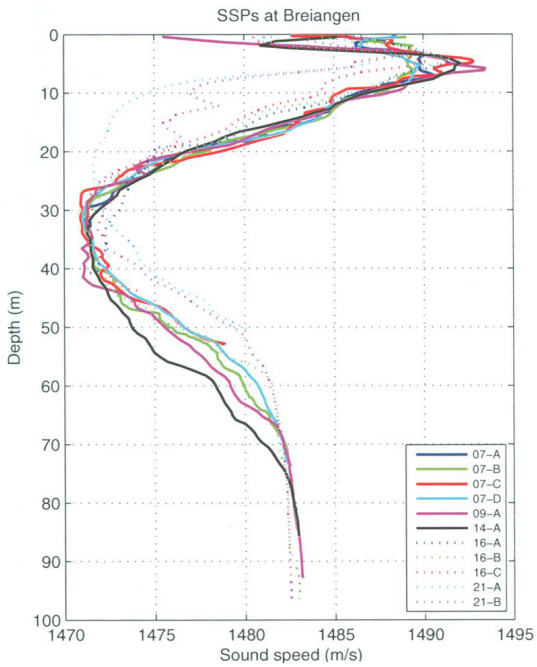

Figure 3.3: The sound speed profile at different locations in Breiangen during the recording over depth, taken from [7].

The a representative of the 09-A recording is used in RAM, because the location of this measurement is in the area of the NILUS-node and is considered to be a good presentation of the SSP during the ship recording. As the SSP is only shown down to 100 meters the sound speed can be considered constant down to 200 meter. The Lloyd mirror assume constant sound speed and when looking at 09-A a reasonable presentation of the sound speed in the water layer will be 1482 m/s.

The bottom properties are found from a sea map from Kartverket, see figure 3.1 and there is marked Cy, Cy M and S at some locations. The marks stands for Clay, Clay and Mud and Sand and some typical values are in table II which have taken it from [14, p. 39]. There is no other known survey of the area and it marks some elevations where the bottom is harder rock, but this can't be considered in the Lloyd mirror model.

The bottom properties can be considered to be clay and mud, there is no specific

Table II: The properties of clay, silt and sand, found in [14, p. 39]

Bottom type	Density (kg/m^3)	Sound speed (m/s)	Attenuation (dB/λ)
Clay	1500	1500	0.2
Silt	1700	1575	1.0
Sand	1900	1650	0.8

value for mud, but it should be somewhere between clay and silt. The top layer is assumed to be dominated by clay, only compressional properties are considered and the sediment properties for the Lloyd mirror model are assumed to be c_s 1502 m/s and ρ_s 1500 kg/m^3. RAM assumes the top layer consists mostly by clay with a depth of 100 meters and the second layer to be mostly mud.

The ship passing over sea floor with almost constant depth will be most suited for the estimation, such as ships coming from Drammen, see sea map 3.1. The depth of the bottom profiles for this passings ranges around 200 meters, which gives the propagation model some uncertainty.

Chapter 4

Method and Results

In this chapter the methods used to process the recored data and the methods used in the inversion problem are described. The results using these methods on synthetic and recorded data is represented and evaluated.

4.1 Method

It is assumed that the ship travels with constant velocity and in a straight path, which is a fair assumption when considering the AIS data in section 3.4. The ship path can then be recreated in time with the horizontal range between the ship and the receiver at the the closest point of approach, d_{cpa}, and the boats velocity, v_s. The horizontal range and ship velocity are unknown and this problem is solved by applying a matched field inversion method, based on the method in [18] with some adjustments and modifications, to estimate this parameters. The methods used on the recored data and in the inversion method are described and discussed in this section.

4.1.1 Matched Field Inversion

The matched field method consists of a propagation model, cost function and a search algorithm. The cost function described in section 2.3 matches the acoustical propagation field of some chosen recorded data with modeled data. The

modeled data are created with the Lloyd mirror model described in the section 2.2 with horizontal range and ship velocity parameters chosen by a search algorithm. The search algorithm determines the parameters in the propagation model and applies the cost function each time and stops when the search algorithms stop criteria has been met. This can be looked at as a loop and is illustrated in section 4.1.3.

4.1.1.1 Propagation model

The Lloyd mirror model calculates the pressure at a certain range and frequency, this value is considered as the Fourier transform at this parameters. To calculate the amplitude from this value, the absolute value is found.

The source used in this thesis is a point source. The source could be looked at as some kind of distributed source, but the Lloyd pattern is clearly visible for the point source. A distributed source is also difficult to predict, because the inversion method should be applied to different ship types and the distribution of the ships are unknown. The Lloyd mirror model isn't considering absorption in the layers either, but this isn't that important as this loss can be considered relative small for the frequencies which are considered (50-1000Hz), when the absorption is 0.4 dB/λ.

In the project a short study was performed on the how accurate the Lloyd mirror model was, where the Lloyd mirror was compared with the RAM model as the synthetic data. The accuracy for good estimation for the model was considered to be around 300 meters. The sound speed profile didn't seem to affect the matched field estimation in a noticeable way and the bathymetry of the sea floor seemed to affect the accuracy of the model for higher range.

4.1.1.2 Construct ship path

The method for creating the modeled data will be established in this section. The cost function isn't using each step in time and in frequency for comparison, that would take a lot of time and use a lot of data when the interesting area of data is the 2 first minutes of the signal from 50-1000 Hz. From the project, the cost function seem only to need data from some frequencies at some points in time to establish how the propagation field are for both sets of data. The measured signal is recorded over time, where both the boat velocity and d_{cpa} are

unknown, but the modeled data can only be change in sense of time by changing the range parameter. The Lloyd mirror model can easily create data for any frequency, but calculating the pressure for a given time is a problem and is solved by reconstructing the ship path, where the assumption of constant ship velocity and straight traveling path is important.

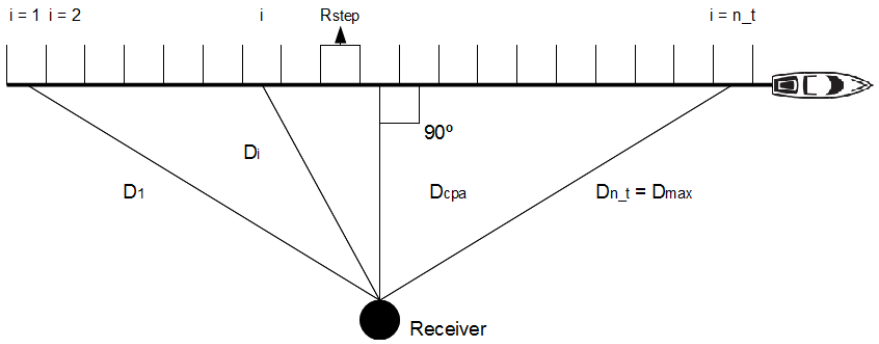

Figure 4.1: Reconstructing ship path, take from the project

The view in the figure 4.1 is from above while the ship is passing by, emitting noise all the time. The figure shows the idea of how the reconstruction of the ship path is done, where i is the number on the time blocks which has been Fourier transformed and n_t is the number of time blocks used. By using the known time interval between each measurement and the d_{cpa}, the range D_i between the source and the i'th time block can be calculated with simple geometry

$$D_i = \sqrt{D_{cpa}^2 + (i \cdot R_{step})^2} \tag{4.1}$$

with the step range calculated as $R_{step} = T v_s$, where T is the length of the of the time block in seconds. The wanted horizontal range is the point in the middle of the time blocks as shown in figure 4.1, but the calculated CPA from the recorded data will be at the start of the time block. This problem can be solved by moving the start of the CPA for the modeled data a half step in the 'after CPA' direction. Because of the bathymetry of the experiment, the ship path is not wanted to be reconstructed symmetrical around the d_cpa as in the figure. There is no problem creating the propagation field with any number of time blocks in either direction, but it has to correspond with which data in the recorded data are used in the estimation.

The tracking of the ship path can be done by using the equation 4.1 to calculated

the horizontal distance when the parameters are estimated. Equation 2.14 in section2.2 can be used to calculate the slant range between the receiver and the ship if this is desired, after some small modifications are made in the equation.

4.1.1.3 Loss and search

There is one thing that is important to know about the cost function when it compares the two sets of data, and that is it checks the ratio between data in the data set and compares this with each other, which results in comparing the change over time and frequency in the two data sets. By subtracting the data set with the average value of the data set, the cost function normalize the magnitude and ensure that the ratio and not the magnitude between the different data sets are compared.

The cost function may prove to give low loss (cost function error) at other combinations of parameters than the real parameters, as was discovered in the project and this is the reason for the thesis to exploring the three different search algorithms: simple 2D search, ASHS (Adaptive Simplex Harmonic Search) and ASDE (Adaptive Simplex Differential Evolution). By using a global search algorithm the application of the method is extended to consider more than two unknown variable, where the 2D search is limited to two unknown parameters. There is no time restriction for the algorithm in this thesis, because the focus of study is to see if the method can find good estimations of the unknown parameters, but may be in focus in future studies.

The simple two dimensional search through the parameter space only need to classify the boundaries of the parameter interval. But the two global search algorithms are a bit more complex, because appropriate control parameters have to be set for the algorithms. A search with good exploration is desired to be sure that the global solution is found on the account of multiple local minimums in the parameter space. These control parameters also depends on the size of the parameter intervals which is searched through. After some trial and error of estimating the parameters, where the Lloyd mirror is compared with it self (no noise synthetic data), the control parameters in table III where found for search over large parameter intervals.

Where the DE starting population is N_{pop}, the crossover constant is CR and amplification constant is F_{weight}. For HS the starting population is HMS, $HMCR$ is the probability of basing the new parameters on the previous, PAR controls

Table III: Control parameters for ASHS and ASDE.

ASHS		ASDE	
HMS	100	N_{pop}	120
$HMCR$	0.4	CR	0.8
PAR	0.4	F_{weight}	0.6
FW	(ub-lb)/50		
$nglobal$	171	$nlocal$	254

rate if adjustment and ub and lb is the upper and lower boundaries of the parameters.

The population is fairly high and the rate of mutation is average, as is the magnitude of the mutation. Large population ensure that the search is done for a large space, but each time it is mutating it's changed with an average magnitude. This parameters balances between exploitation and exploration of the parameters space. The stop criteria is a minimum loss tolerated, this value is not adaptable and will not change as the search for the best solution goes on. In case the search algorithm doesn't find sufficient low estimates, a max number of cost function runs is set for both the global and local part of the adaptive simplex global algorithms, $nglobal$ and $nloca$, which gives the algorithm a lot of time to find a good estimate.

4.1.2 Process recorded data

The recorded data are a discrete signal and by using the signal processing method in section 2.1, the data which is needed in the cost function can be extracted. For the measured data to extract time and frequency data the time signal has to be separated into certain time lengths, by Fourier transform this time blocks with the FFT function in MATLAB the signal will be represented in both time and frequency domain.

Before any values can be taken out of this propagation spectrum, the CPA has to be found. This is done the same way as in [18, p. 944], where the amplitude value for all the frequencies is summed at each time block and the point with the highest value is the CPA. The recorded data has some clipping, which makes finding the point of highest value at the CPA hard. Instead the area with a large amount of high values are found and the CPA is found by a search through this area for the highest value. Each time block is sampled at a given rate and as long

as the process for finding the right values of the measured data corresponds to the modeled data, see 4.1, there will be no problem choosing values around the CPA.

This signal will have a lot of variance, because the signal is ship noise, which can be reduced with the welch spectral estimation method. The frequency resolution will be sacrificed in this process so how much information is lost in the spectral estimation has to be considered. The resolution must be high enough that the propagation pattern is visible, otherwise the inversion method may not find good estimations. It is also preferred that the averaging method gives frequency bands of 1 Hz for a sufficient representation of the propagation over both frequency and range. The chosen frequencies and time blocks can be extracted from the data set after the amplitude of averaged data set are calculated.

4.1.3 Overview

The methods described in 4.1.1 and4.1.2 are presented by a step by step block diagram for an easy and graspable overview of the system.

Where the recorded signal is sent for processing and the predetermined parameters are feed to the signal processing and matched field inversion. When the process is done it returns the best estimated parameters found.

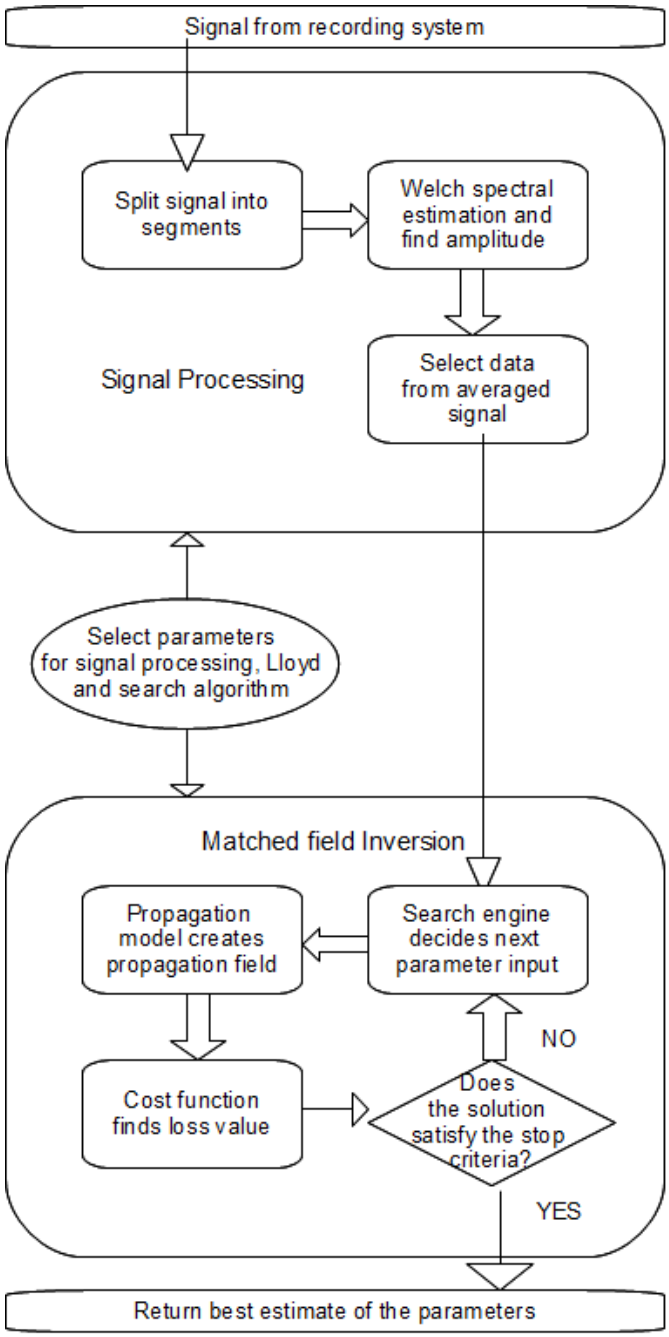

Figure 4.2: A step by step block diagram of estimation method.

4.1.4 Noise

In this section the noise contribution of the ocean is discussed for creating synthetic noisy data and a method for estimating the ships source depth is presented.

4.1.4.1 Ambient Noise

Ocean ambient noise is complex and random. The noise is it is related to area of the sea, weather conditions and the frequency and most of the contributions is shown in spring [5]. The contribution of rain is very high for shallow water, but there is no or little rain during the recordings as discussed in section 3.5 and will therefore not affect the the signal. The ship noise is supposed to be the signal and is discussed in section 4.1.4.2. Then the ambient noise may be considered to be mainly a contribution of turbulence, wind and thermal noise for the relevant frequencies. The power of the noise can be calculated by the formula taken from [1]

$$\begin{aligned} N_t &= 17 - 30log(f) \\ N_w &= 50 + 7.5w^{1/2} + 20log(f) - 40log(f + 0.4) \\ N_{th} &= -15 + 20log(f) \end{aligned} \tag{4.2}$$

where N_t is the noise contribution from the turbulence, the N_w is from the wind, the N_{th} is thermal noise and w and f is the wind speed and frequency. This is the noise used in testing the method for noisy data.

4.1.4.2 Ship Noise and source depth

The ships noise is emitted at frequencies up to 10 kHz, but the bandwidth of the noise depends on the ship and for commercial ships the frequency is known to peak at 50 - 150 Hz. To cower the most important frequencies the bandwidth can be considered approximately to be 50 -1000 Hz, from [16]. Surface vessels radiates noise in a complex way and the underwater noise emitted from the ship comes mainly from

- The propeller
- The propulsion machinery

- The hydraulic flow over the hull

The main source of noise is the propeller and account for around 80-85 % of the ship-radiated noise power, where the noise comes from cavitations. The propeller creates both broadband and tonal noise, which comes from the blade frequency and their harmonics. It's then appropriate to say that the source localization would be close to the propeller. The effective source depth can then be considered to be the ships depth minus 85 % of the propeller diameter and is defined as

$$d_s = D - 0.85P \tag{4.3}$$

where D is the ship draft and P is the diameter of the propeller, from [27, p. 1231]. If no data about the propeller is available, a provisional method may be to set the propeller diameter as half the ship draft.

$$P = \frac{D}{2}. \tag{4.4}$$

The source depth are be difficult to determine, because the draft and depth of propeller variates from ship to ship and their cargo. This is just an estimation of the source depth when including that the draft is unknown and only a mean value is provided.

4.2 Ship information

The required ship information is listed in table IV, such as ship name and type, the location of the recording, the speed of the vessel, the distance at the CPA from the AIS data and the average draft. The average source depth is calculated from the draft using formula 4.3 and 4.4, where the information of the propeller of the vessel is unknown. The information of the recordings for the ships are in table V, where the time at CPA from start of time sample, the time sample length, start and end, the date of the recording was done and the direction the boat was traveling in.

Table IV: The ships name, type, location of the recording, speed, distance at CPA and average draft.

Time sample	Ship name	NILUS location	Ship-type	Ship velocity (knots)	Distance at CPA (m)	Draft (m)	Mean source depth (m)
Sample 1	Småen	A	Tender	14	3.75	3.1	1.8
Sample 3	Jumbo	A	Cargo	5.5	65	5.5	3.2

Table V: The time information of the recordings and the direction the ships are traveling in.

Ship name	NILUS location	Time at CPA (min)	Length of recording (min)	Start of signal	End of signal	Date	Start position	End position
Småen	A	06:48	15	09:51	10:06	18.06	R2W	R2E
Jumbo	A	04:52	20	15:38	15:58	17.06	R2W	R2E

4.3 Received data

In this section the recorded data has been processed and is presented with an example of the Lloyd model propagation data.

The received data is processed as described in the section 4.1.2. The signal is separated into segments of 1 seconds and the welch spectral estimation method is used on this segment to reduce the variance. The length of each segment is 9000 samples and a 9000 points fast Fourier transform is used to yield the frequencies such that the amplitude and PSD can be calculated for each 1 second time block. The amplitude values are summed at each time block to find the time of CPA.

The welch function separates the 1 second time block in 3 segments with 50 % overlapping, but the pwelch method uses the closest number of samples from bellow of the factor of 2 for this process, which yields a $\Delta f \approx 1$.

The two time signals are chosen because of the high SNR which makes the Lloyd mirror pattern visible. The raw data of the two boats are shown in appendix B.1.

4.3.1 Jumbo at NILUS-A

In this section the results of the signal processing of at NILUS-A for the Jumbo passing are shown.

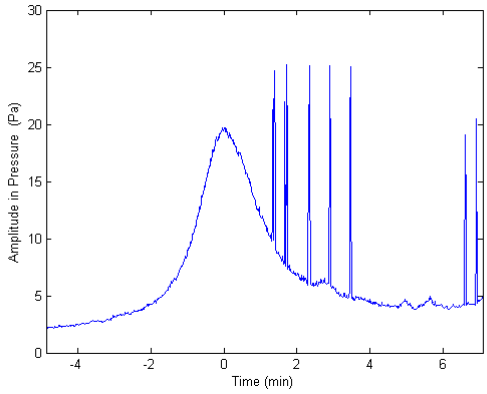

Figure 4.3: The sum of amplitude value over frequencies at each time block of Jumbo.

Figure 4.3 shows the sum of the amplitude values over the frequencies for each time block. This shows that the point of CPA is at 04:52 after the start of the time sample. There occur some clipping from the internal communication device on the NILUS-sensor at more than one point after the CPA and it's important not to select this time blocks in the matched field method. The bathymetry before CPA is more or less flat as mention in chapter 3, which is in agreement with choosing data before CPA.

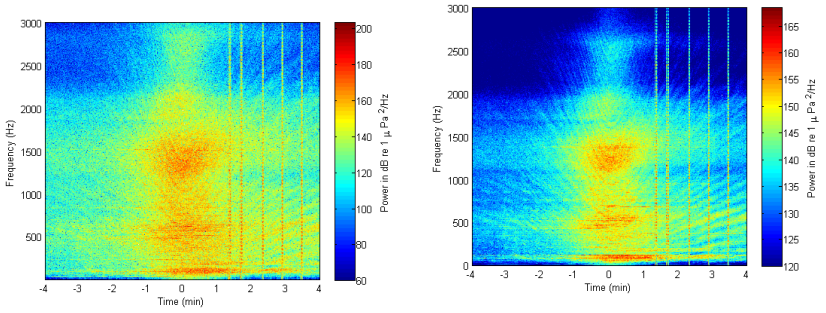

(a) The PSD over time and frequencies.

(b) The welch estimation over time and frequencies.

Figure 4.4: PSD and welch spectral estimation of Jumbo over frequency and time.

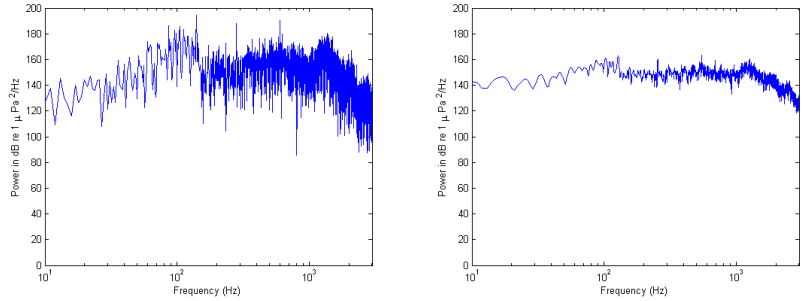

(a) The PSD at CPA.

(b) The welch estimation at CPA.

Figure 4.5: PSD and welch spectral estimation over frequency for the time block at CPA of Jumbo.

The figure 4.4 shows the PSD compared with the welch spectral estimation of the signal over time and frequencies and in figure 4.5 the propagation over frequencies is taken out at CPA to study further the effect of the welch estimation. Only

the 4 first minutes before and after the CPA are shown, because the matched field model only selects data up to 3 minutes away from the CPA, due to the fact that data beyond this point has low SNR. The minimum level is caped in the figures at 60 dB for the PSD and 120 dB for the welch estimation, which is done to make the Lloyd mirror pattern more visible. The PSD have lover limit to better show the propagation pattern close to the CPA.

The time of CPA is not quite perfect as can be seen especially in figure 4.4a and some in figure 4.4b, because the CPA might be a bit more to the right of the CPA where the propagation pattern seems to start. This is an error which has to be taken into consideration when looking for good estimation of the parameters. The propagation pattern is visible, especially in figure 4.4b over longer range, which makes it more likely a good estimation of the parameters can be found. The magnitude of the power level of the recorded signal seems to be very high, but may be because the ship is traveling considerable close to the receiver and the ship traffic in the area might have contributed to this levels.

The figures shows that the variance and SNR increases with the frequency and the welch estimation lower the variance considerably. It is highly apparent in the figures 4.5a and 4.5b that the levels are smoothed for low frequencies. The variance is still a bit high for frequencies above1 kHz after welch estimation, but for the relevant frequencies (50-1000 Hz) the variance is considerable lower.

Another observation is that the recordings after the CPA, even if it is moved a bit to the right, are stretched out over time compared to the data before the CPA. This is very visible when looking at the raw time sample in figure B.1a in appendix B.1, and is most likely caused by propagation effects.

4.3.2 Småen at Nilus-A

In this section the results of the signal processing of at NILUS-A for the Småen passing are shown.

The amplitude values over the frequencies is summed to find the closest point of approach as shown in figure 4.6. The CPA occur at 06:48 after the start of the time sample. Unlike Jumbo, Småen has a lot of clipping in its signal which makes it hard for the time block selecting algorithm, because the data with clipping are useless in the matched field method. The best time blocks are before CPA because of the bathymetry for småen as for Jumbo, but there are 3 areas with clipping before the 3 minutes mark. The clippings are avoided by making the

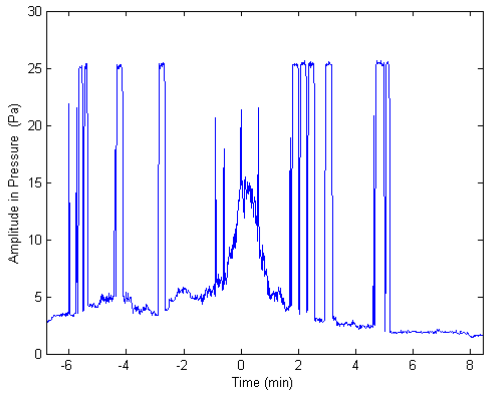

Figure 4.6: The sum of amplitude value over frequencies at each time block of Småen.

algorithm doing the signal processing not choose these time blocks.

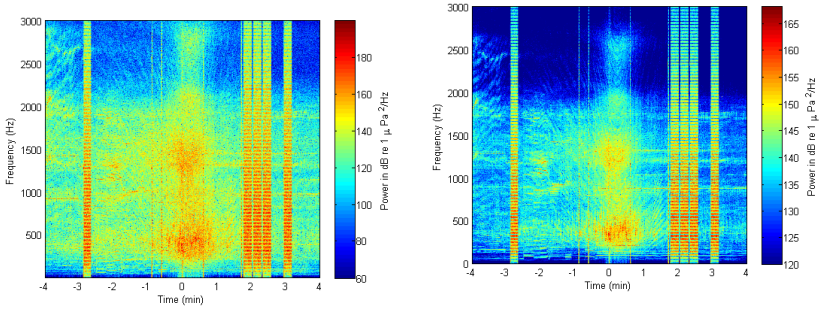

(a) The PSD over time and frequencies.

(b) The welch estimation over time and frequencies.

Figure 4.7: PSD and welch spectral estimation of Småen over frequency and time.

The figure 4.7 shows the PSD compared with the welch spectral estimation of the signal over time and frequencies and in figure 4.8 the propagation over frequencies is taken out at CPA to be studied further. The propagation is shown for the same time and frequencies as Jumbo.

The detection of CPA had some problem for Småen as the Jumbo sample, which can be seen from the figures 4.7 and 4.6, but the Småens CPA is found close to

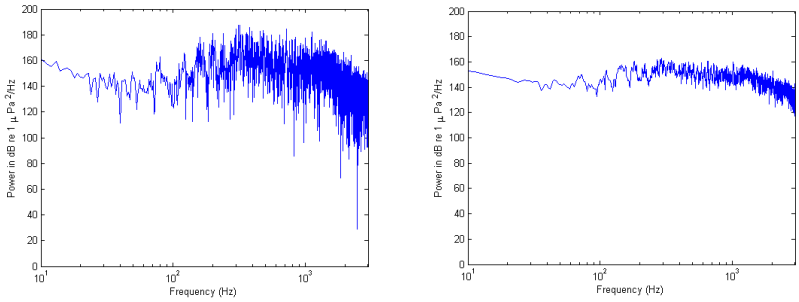

(a) The PSD at CPA.

(b) The welch estimation at CPA.

Figure 4.8: PSD and welch spectral estimation over frequency for the time block at CPA of Småen.

one of the clippings close to the CPA. The CPA may be a bit after the current CPA where the propagation pattern seems to start and where the highest value is, when not considering the areas with clipping. The error of CPA at Jumbo can be considered to be manageable, but it's not advantageous to have the CPA at data with clippings, so this is solved by just manually move the CPA a bit to the right of the CPA for the Småen case to avoid clipping. This is an error which has to be taken into consideration when analyzing the results of the matched field inversion. The Lloyd mirror pattern is visible, as can be seen in figure 4.7b, which makes it likely a good estimation of the parameters can be found.

From figure 4.7b there seems to be another ship passing by around 4 minutes before CPA, but this seems to occur at the same time as Småen changes course when considering the recorded AIS distance in figure 3.2a, which makes it plausible that this pattern is made by Småen. There are no visible change in the recording to say that this affects the passing of Småen at CPA, but it is hard to say with all the clippings and might be necessary to take into consideration when looking for good estimations. Time blocks further away than 2 minutes should be avoided for the matched field method to ensure that this doesn't affect the estimation and to avoid clippings. The magnitude of the power of the recorded signal seems to be high for this recording too and may be of same reasons at mentioned for Jumbo.

The Småen passing seems to take a shorter time than Jumbo which is easily explained by a higher ship velocity, but this cause the propagation pattern to change more rapidly over time than for Jumbo which can be seen in figure 4.4b

and 4.7. This combined with lower SNR makes the propagation pattern to be less visible than for Jumbo.

Småen seems to suffer from a little more variance than Jumbo and even if the welch reduces this considerably the variance is still visible for higher frequencies than 1 kHz after welch estimation. The relevant frequencies (50-1000 Hz) seems to have low enough variance for the matched field method. It is very apparent when comparing the figures 4.5a and 4.8b that the levels are smoothed for low frequencies like the Jumbo case.

4.3.3 Example of propagation model

To illustrate the propagation field an example of the third order Lloyd mirror and Ram is made based on the data from Jumbo. The purpose is to see the comparison between propagation field for the models and to compare it with the recorded propagation field.

Table VI: The parameters used in the example of the Lloyd mirror and RAM propagation model.

Shared		Lloyd mirror		RAM			
f	1 - 3000 Hz	c_w	1482 m/s	SP	09-A	$\rho_s 2$	1800 kg/m^3
d_s	3.2 m	c_s	1502 m/s	$c_s 1$	1500 m/s	$\alpha_s 1$	0.2 dB/λ
d_b	200 m	ρ_w	1000 kg/m^3	$c_s 2$	1615 m/s	$\alpha_s 2$	0.9 dB/λ
d_w	200 m	ρ_s	1500 kg/m^3	ρ_w	1000 kg/m^3	d_c	100 m
r	1 - 3000 m	L_o	3	$\rho_s 1$	1500 kg/m^3		

The parameters necessary for creating the Lloyd mirror and RAM propagation fields are listed in table VI. The table is separated into parameters which is shared in both models, exclusive Lloyd mirror model parameters and RAM parameters, where L_o is the order of the Lloyd mirror model, SP is the sound speed profile, $c_s 1$ and $c_s 2$ are the sound speed in the sediment in the middle and bottom, $\rho_s 1$ and $\rho_s 2$ are the density in the sediment in the middle and bottom and the d_c is the depth of the first sediment layer. The rest of the parameters are described in the theory chapter 2. The RAM model is considering two homogeneous layers in the ocean floor and the sound speed profile 09-A as described in the environmental data section 3.5.

The propagation fields are shown in figure 4.19 and are displayed as transmission loss over range and frequencies with a reference of 1 mPa as described in

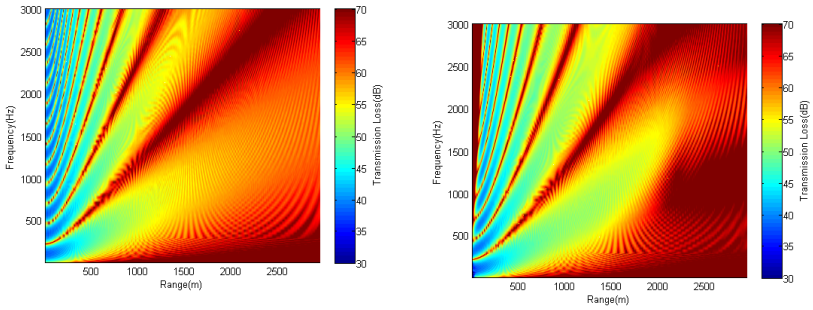

(a) The third order Lloyd mirror propagation field.

(b) The RAM propagation field.

Figure 4.9: Example of propagation field over range and frequencies, created by the Lloyd mirror and RAM propagation models.

the theory. Both RAM and the Lloyd mirror models are range and frequency dependent as the figures shows. The propagation field made by RAM and the third order of Lloyd mirror seem to be closely matched at short range and slowly differs as the range increases as described in the project, but it's a bit difficult to see the details in these figures.

4.4 Estimation of noisy synthetic data

In this section synthetic data with added noise is matched with modeled data to see how the method behaves for ideal noisy data. The limitations of the method when facing a noisy signal is useful when analyzing the recorded data.

The Noise is constructed from the equations 4.2, which gives a good estimation on how ambient noise is distributed over the frequencies. The noise is added to the signal in three steps. Firstly the noise and the synthetic propagation field without add noise are created. Secondly the created noise is scaled in comparison with the synthetic data at CPA in dB. The scaling is done by first take the average amplitude value over the chosen frequencies for the constructed noise and the synthetic data, to preserve the frequency distribution, and find the value which will adjust the noise to the desired level of SNR. This is done with the formula $N_{adj} = \frac{A_s}{A_n 10^{SNR/20}}$, where the N_{adj} is the constant which the noise will be adjusted with, the A_s and A_n is the mean value of the synthetic data and the noise and SNR is the signal to noise ratio that is desired in dB. This formula is

modified from the formula for power in [29, p. 20] when considering the amplitude value. The noise is adjusted and will be the mean value of the distribution of the noise with variance around this mean. For example, with a variance of 1, the mean value will alter with a magnitude equal to the mean value in either direction. The variance is created by using the *randn* function in MATLAB, which has a gauss distribution. The third step is adding this noise to the different frequencies for all the data in the synthetic propagation field.

Table VII: The parameters used in creating the synthetic data.

t_{len}	1 s	f	100 200 400 600 800 Hz	c_w	1500 m/s
t_{bet}	5	d_s	2.2 m	c_s	1700 m/s
w	4	d_b	200 m	ρ_w	1000 kg/m^3
L_o	3	d_w	200 m	ρ_s	1900 kg/m^3
sbal	2	d_{cpa}	250 m	v_s	10 knots
		d_{cpai}	100 - 500 m	v_{si}	2 - 20 knots

The necessary parameters for creating both synthetic and modeled data are given in table VII, where t_{len} are the length of the a time block in seconds, t_{bet} are number of time blocks spacing between each time block used and t_{num} are the number of time blocks used, this are time parameters which decides which amplitudes from the propagation field which are used in the matching. The d_{cpai} and v_{si} are the boundaries for the unknown parameter d_{cpa} and v_s that are used in the search algorithm. The other parameters have already been discussed in the theory chapter 2 or in section 4.1, except the parameter $sbal$, which decided how many time blocks in the one direction of the CPA are used, the rest of the time blocks are then on the other side of the CPA. The direction of the $sbal$ depends on which direction is believed to result in good estimations. The direction is of no relevance for the synthetic case, because both synthetic and modeled data are created with the Lloyd mirror model and is symmetric around CPA.

The estimation of the synthetic data is done by comparing the synthetic data, which is a Lloyd mirror model of order 5 with added noise, with the modeled data which is order 3. Both models uses the same parameters in table VII, except of the d_{cpa} and v_s, which are replaced with the boundaries in creating the modeled data. The study then can be divided into testing low SNR and high variance in the noise, low number of time blocks and how the global search algorithms was handling noisy data. The number of frequencies has already been studied in the project.

4.4.1 Low SNR and high variance

Low SNR and high variance is studied first and the t_{num} is set to be constant while different values of SNR and variance is tested, the noise is random generated for each case.

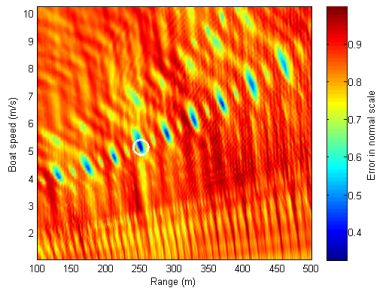

(a) Result of a bit lower SNR and high variance.

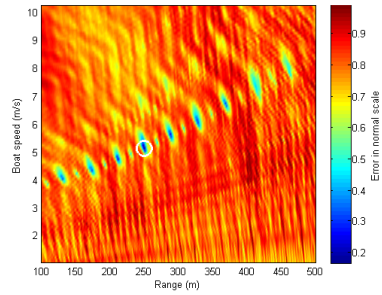

(b) Result of low SNR and average variance.

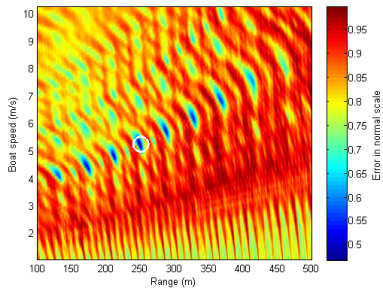

(c) Result of very low SNR and average variance.

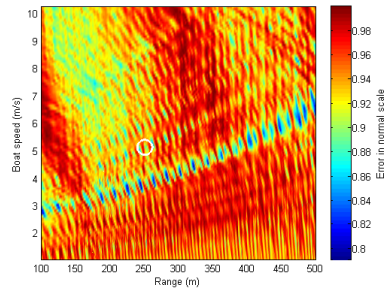

(d) Result where the noise is dominant, but low variance.

Figure 4.10: 2D search of synthetic data, plotting the cost function error at each combination of the parameters with normal scaled loss. The SNR and variance of the noise are changed between each figure with t_{num} 24, where a SNR of 10 dB is considered on the edge of good SNR, see table IX for the estimated parameters and the noise used in the estimation.

The plots in figure 4.10 shows the 2D search algorithm in normal scale with different SNR and magnitude of variance. It is shown in normal scale because it was hard to see some of the areas with low loss with dB scale and the error value are of interest.

Table VIII: The estimated parameters of 2D search with noisy synthetic data from the figures in 4.10.

Figure	Estimated ship velocity (m/s)	Estimated hor. range (m)	t_{num}	SNR (dB)	variance
4.10a	5.12	251	24	5	1.0
4.10b	5.12	250	24	0	0.3
4.10c	5.23	251	24	-5	0.5
4.10d	5.12	251	24	-40	0.1

It seems to be a pattern of low loss almost linear with rising parameter values. This pattern of potential good estimations also seem to be dependent on the magnitude of the SNR and the variance. High variance increases the number of such patterns and visa versa, when considering the figures in 4.10. High difference in the magnitude between the compared models also creates more areas with seemingly good estimates, but is a little displaced in the parameter space. First of we have the variance which creates more such areas or rather makes them more visible. This can be explained by that there exist combinations of parameters which creates propagation patterns which are to some extent similar to the synthetic propagation pattern. By looking at the Loyd propagation field in figure 4.9a in section 4.3, the similar propagation patterns are repeating it self at different range and frequencies and it is not unthinkable that the normalized ratio gives low loss for them. When some variance is added to the synthetic propagation pattern the low loss pattern will change and will give higher loss when using the cost function. So compared with the other similar patterns, the synthetic pattern isn't that different anymore, which creates the pattern of good estimates. If the variance is high enough, another set off parameters might be considered the best estimation, because the variance changes the synthetic propagation pattern so much it almost can't be distinguished from other similar propagation patterns. The high number of this low loss patterns might be because the d_{cpa} is fairly high and close to the limitation of the Lloyd mirror model.

High difference in the magnitude between the two data sets creates high loss, as shown in figure 4.10d, and the low loss pattern is displaced in the parameter space. The reason for the displacement to lower velocity seem to be the combination of high noise and some variance, which cause the cost function recognize it as another part of the propagation field. The variance is high for low SNR because it is scaled with it and this creates very high loss for all parameters in the

parameter space, 0.8 as a minimum, which makes the areas with low loss seems to point to wrong parameters. The search in figure 4.10d still finds the correct parameters even though it doesn't look it when studying the figure. However, this is synthetic data and not data from a real recording, consequently, it will create a perfect propagation field as a basis.

A limit to low SNR doesn't seem the be present, as it is further shown in figure B.2d in appendix B.2. The matched field inversion finds the correct parameter values as long as there is no or low variance in the noise compared with the amplitude value, even though it finds other areas with low loss and has generally very high loss as in figure 4.10d it recognizes the ratio of the values and finds the correct parameters. When adding variance to the noise there is a whole other matter and the propagation field is not as easily recognized. The variance magnitude is changing with SNR and which doesn't make pinpointing the limitation very easy, but variance usually depend on the magnitude of noise so it's not a bad approximation. This is why it is important to reduce the variance in the recording.

4.4.2 Low number of time blocks

Different numbers of t_{num} with different variance is tested to find the lowest number of time blocks which could be used, where the SNR is set to 10 dB.

Table IX: The estimated parameters of 2D search with noisy synthetic data from the figures in 4.11.

Figure	Estimated ship velocity (m/s)	Estimated hor. range (m)	t_{num}	SNR (dB)	variance
4.11a	5.12	250	12	10	1.0
4.11b	5.43	289	10	10	1.0
4.11c	5.12	250	8	10	0.3
4.11d	7.12	435	6	10	0.3

In the figures in 4.11 there is present a new pattern which was only partly visible in the figures 4.10c and is very visible for low number of t_{num} as shown in figure 4.11d especially. This pattern is created when searching through low values of ship velocity and can be explain by that the low number of time blocks around a point looks very similar to any other point because the pattern around isn't explored thoroughly. The ship velocity decides how far the boat has traveled

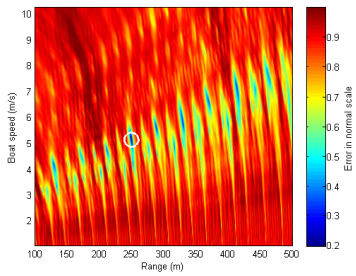

(a) Result of a bit lower t_{num} and high variance.

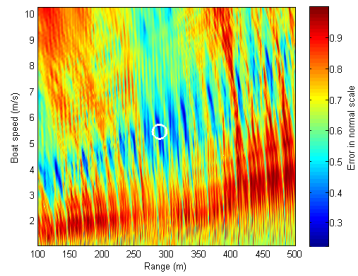

(b) Result of low t_{num} and high variance.

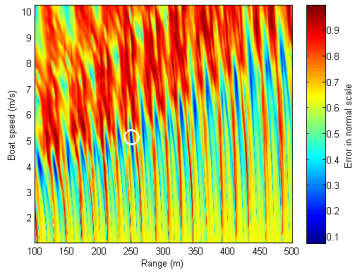

(c) Result of even lower t_{num}, but average variance.

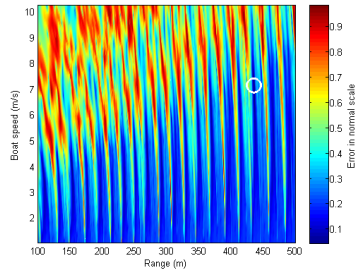

(d) Result of very low t_{num} and average variance.

Figure 4.11: 2D search of synthetic data, plotting the cost function error at each combination of the parameters with normal scaled loss. The t_{num} and variance of the noise are changed between each figure with SNR 10 dB, where a t_{num} of 16 is considered on the edge of enough data, see table IX for the estimated parameters, noise and parameter used in the estimation.

at each time block and higher boat speed mens larger areas which is explored, which is very important when handling low number of time blocks.

Another observation, which isn't very clear from the figures in 4.10 and 4.11, is that by increasing t_{num} the higher the error is generally. This occur only for variating data and is caused by the fact that the error of the cost function is calculated by the ratio between the two fields. The cost function will return high error when matching a lot of values with low variating noise compared to less values with the same low variating noise, because it is more data to find error in as can be seen when comparing figures 4.11a and 4.11b. The method will be more accurate with high t_{num}, but all combinations of the parameters will generally return

higher loss. On the other hand the SNR is highest at CPA and a very large number of time blocks may not be an advantage if it uses data with no traces of the signal left in it.

The limitation of t_{num} isn't easily found, because it varies with the variance just like the limitations of the SNR. The figure 4.11c shows, the method can find good estimations for low number of time blocks as long as the variance is low, but should be sufficiently high to ensure that the low loss pattern doesn't affect the estimation of the parameters. This pattern seems to move up the velocity parameter as the range increases, so when considering large range intervals a sufficiently high number of time blocks should be considered.

4.4.3 Global algorithm

Both the global algorithms, ASHS and ASDE, is used in the estimation to see how the quality of the estimations both of them can produce. They are set to run 10 times with a new generated noise for each iteration to see if they only finds one set of parameters or finds other sets.

Table X: The mean estimated parameters of the global algorithms for noisy synthetic data from the figures in 4.12.

Figure	Global algorithm	Mean ship velocity (m/s)	Mean hor. range (m)	t_{num}	SNR (dB)	variance
4.12a	ASHS	5.32	260	14	10	1.0
	ASDE	5.32	257	14	10	1.0
4.12b	ASHS	5.18	250	24	5	1.0
	ASDE	5.18	240	24	5	1.0
4.12c	ASHS	5.23	260	24	5	0.5
	ASDE	5.23	257	24	5	0.5

The stop criteria is a minimum value of the error returned from the cost function and, as the figures in 4.10 shows, this stop criteria has to be changed with the case presented to find the correct estimation of the parameters. This value should preferable be set to the error at the correct parameters, but without knowing the parameters this value is hard to guess when presented with a number of areas with low loss. The global algorithms are very fast at finding estimation which fulfill the criteria, so the procedure used to find this criteria was just simply trial and error starting with a high error value and run the global algorithm until it

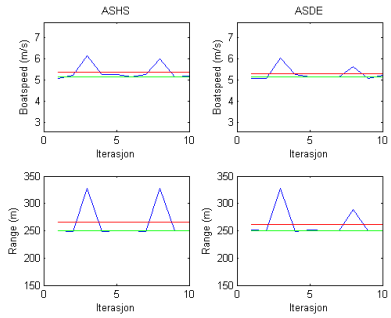

(a) Result with good SNR, high variance and low t_{num}.

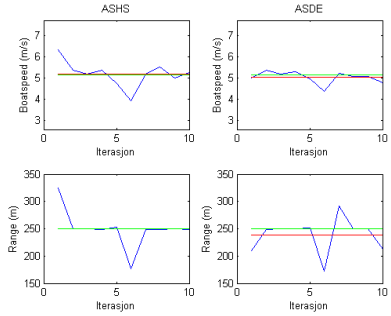

(b) Result with low SNR, high variance and high t_{num}.

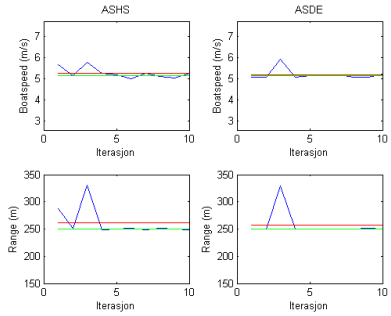

(c) Result with low SNR, average variance and high t_{num}.

Figure 4.12: ASHS and ASDE search of synthetic data, the blue line is the estimated value, the red the mean value of the estimates and the green line is the real value. The t_{num}, SNR and variance of the noise are changed between each figure, see table X for the estimated parameters and the noise and parameter used in the estimation.

starts to use a long time to find a good estimation. When one of the global algorithms are using long time it either have problem finding parameters that fulfill the stop criteria (if there are any), or the parameter space which it's searching through are very large, or the algorithm has been very unlucky with the start population and it uses some time to find the global minimum, or it's stuck in the a local minimum loss area and the mutation in the global algorithms isn't doing its job. Another way of finding an agreeable stop criteria error is to either use the simple 2D search to find the areas with good estimations or set the stop criteria very low and run the global algorithm once. This will make the algorithm stop only by the reaching the maximum number of function calls and will find lowest loss possible in the parameter space, but both of this methods takes a lot of time compared with trial and error. On the other hand if two areas with almost equal loss is presented it will be hard find the best stop criteria with trial and error.

The figures in 4.12 shows both parameters when using ASHS and ASDE for 3 different cases with the estimated parameter, average of the estimated and real value of the parameter. The algorithm doesn't always find the correct parameters as shown in the figures, which indicates that the error of the stop criteria can be a little lower. For the estimations with low deviation from the real value is searching in the correct area of low loss, but stops on the way to the absolute minimum and this indicates that the search algorithm needed a little more time before the correct parameters was found and the stop criteria should be lower. The estimations which isn't close to the real value are found because the algorithm is stuck in a local low loss area and finds a good enough loss to fulfill the stop criteria. New estimations could be found by lowering the stop criteria, but it is interesting to see how good the algorithms is at finding the correct parameters without perfect stop criteria.

The global search algorithm seems to be more sensitive of large variance than the simple 2D search, which is caused by an uncertain stop criteria. When the variance is high the general error is higher which increases the chance of finding another area with low enough loss to fulfill the stop criteria, as described before. The fact that a new noise is generated at each iteration opens the possibility that the data sett is especially variating in the iterations that estimates the wrong parameter values. This is also observed for the 2D search, where some estimations give parameter values that isn't corresponding well with the correct values and has generally higher loss in the parameter space than the given SNR and variance would normally imply. The global algorithm seems also to be a little more sensitive to the number of time block used, but this is most likely caused by the low loss pattern a small t_{num} creates and random noise.

The error of the parameters and cost function of the figures 4.12 is found in appendix B.2, where more result of the simulations of both simple 2D search and the global algorithms can be found.

4.5 Estimation of recorded data

In this section the matched field inversion method is used to estimate the parameters of the recorded data. The 2D search is used first to analyze the area of loss and the ASHS and ASDE is used on the recording with the source depth d_s as an additional unknown parameter.

Table XI: The parameters which are used to create the modeled data.

Lloyd mirror			
f	100 200 300 500 600 800	c_w	1482 m/s
L_o	3	ρ_w	1000 kg/m^3
d_b	200 m	d_w	200 m

The parameters given in table XI is based on the environmental data in section 3.5. This parameters are the basis in the Lloyd mirror model and the other parameters are changed to find a better estimation. There are six parameters which are frequently changed to find estimations which matches better with the real values. This parameters are the frequency values, d_s, t_{num}, t_{bet}, c_s and ρ_s. The real value for this parameters are not certain, but a basis for the values are taken in the project and chapter 3.

This frequencies are found by analyzing the spectrum of the ship recording and find areas where frequency values have good SNR and have a visible propagation pattern. Different frequencies in this areas are tried out and are given in the following sections. It is desired that the frequencies are spread out over the interval 50 - 1000 Hz.

The rest of the parameters was chosen with trial and error by using the knowledge of how they affect the propagation field and the experience from the project.

The recorded AIS data are assumed to be the real values of the unknown parameters and are given in table IV.

4.5.1 Jumbo at Nilus-A

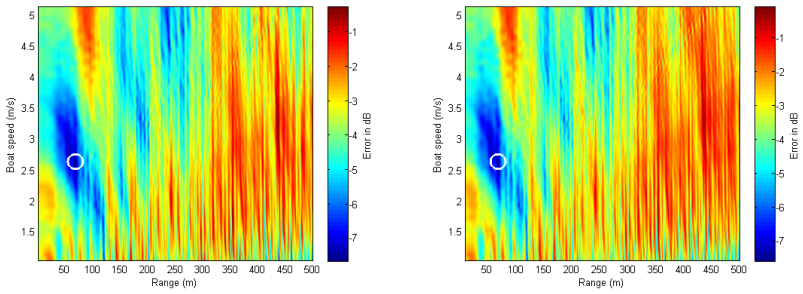

(a) Result with almost the expected set of parameters with medium search intervals.

(b) Result with high bottom properties with medium search intervals.

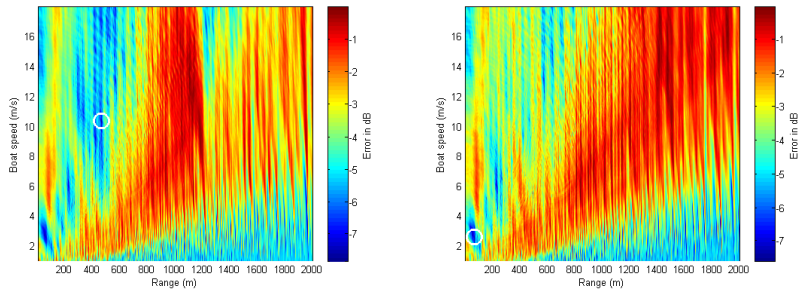

(c) Result with almost the expected set of parameters with large search intervals.

(d) Result with high bottom properties with large search intervals.

Figure 4.13: 2D search of Jumbo, plotting the cost function error at each combination of the parameters with log scale loss. The t_{num}, t_{bet}, d_s, c_s, ρ_s and the search intervals are searched for good results, see table XII for the estimated parameters and parameters used in the estimation.

The 2D search of the recorded signal of Jumbo at NILUS-A is given in figures 4.13 and the estimated parameters of the figures are given in table XII. These plots are given in dB scale, because the areas of low loss will be more visible and the cost function error isn't in the same focus as the synthetic data analyzes. The log scale is calculated with $E_{dB} = 20log(E)$. The figures presented are the best estimations which was found for different combinations of parameters. Further exploration of the parameter space is shown in appendix B.3.1. The data is selected with a chosen number of t_{num} and t_{bet}, where *sbal* is 2 after CPA and the rest are before. This is done because the position of the CPA accurate and it is desired that values close to the CPA should be in the estimation to ensure high SNR for the recorded data, the rising bathymetry will most likely not affect

Table XII: The estimated parameters of 2D search with error of Jumbo from the figures in 4.13, including the parameters to create them.

Figure	Estimated ship velocity (m/s)	Estimated hor. range (m)	Error	v_{si} (m/s)	d_{cpai} (m)	d_s (m)	t_{num}	t_{bet}	c_s (m/s)	ρ_s (kg/m^3)
4.13a	2.63	69	0.4130	1.0-5.1	10-500	3.325	24	3	1516	1520
4.13c	10.33	469	0.4054	1.0-18.0	10-2000	3.325	24	3	1516	1520
4.13b	2.63	69	0.4165	1.0-5.1	10-500	3.325	24	3	1575	1700
4.13d	2.63	69	0.4165	1.0-18.0	10-2000	3.325	24	3	1575	1700

Table XIII: The mean estimated parameters from global algorithm search with error of Jumbo from the figures 4.14 and 4.15, including the boundary condition of the searched parameters and using the same properties as 4.13a.

Figure	Global algorithm	Mean ship velocity (m/s)	Mean hor. range (m)	Mean source depth (m)	Error	v_{si} (m/s)	d_{cpai} (m)	d_{si} (m)
4.14	ASHS	2.63	69	3.3	0.4113	1.0-5.1	10-100	2.6-3.8
	ASDE	2.63	69	3.39	0.4113	1.0-5.1	10-100	2.6-3.8
4.15	ASHS	3.20	118	3.70	0.4183	1.0-5.1	10-500	2.6-4.2
	ASDE	2.83	100	3.49	0.4135	1.0-5.1	10-500	2.6-4.2

the propagation in a significant way because of the low boat speed and low number of time blocks in this direction. Some estimations with *sbal* 0 time blocks after the CPA was done, but they gave a slightly larger cost function error and other parameters.

There is an area around the parameter values found by the AIS with low loss. The area stretches for about 15 meters in either direction and 0.75 m/s up and down in the boat speed parameter. This area is quite large and there are two separate minimum values of the loss in this area which creates some uncertainty when searching for the least loss estimation. At least it seems like this area is more or less the largest in the parameter space and makes it easy for the search algorithms to find it.

There are made some observations of how the error in the parameter space is changing with the different parameters. Change in frequencies change both error and the the location of the areas with low loss in the parameter space. The figure 4.4b, shows that the frequency values bellow 80 Hz might not represent the propagation field in a good way. There are different frequency values which have the same high value over long range as frequency 128 Hz and is therefore avoided, seems like some kind of frequency clipping. There are values around 100 and 500 Hz with high SNR and is important in the matched field inversion. The frequencies 103, 308, 476, 550, 720 and 890 Hz are found to give good results and is used for all the results presented in this section and in the appendix B.3.1.

The source depth given in table IV is close to the one that is found to give the best estimations of the parameters. This parameter is found to be change the estimation a lot and is a important factor for finding good parameters. This is caused by that the whole propagation field is changed and moved in range when the source depth is changed.

The density and sound speed in the bottom element doesn't seem to move the areas of low loss much, but has more affect on the magnitude of the error at the different areas for the Jumbo recording, which will alter the areas with least loss, especially for a search over large intervals. These parameters changes the reflection coefficient, which changes the magnitude of the propagation at longer range. As the figures 4.13b and 4.13d shows and is further explored in the figures in 4.13 and B.8 in appendix B.3.1, the c_s and ρ_s are increased to 1516 m/s and 1520 kg/m^3 to find estimations which corresponds well with the real parameter values, when considering medium sized intervals. The values of 1516 m/s and 1520 kg/m^3 are adequate possibilities, because the clay may not be as dominant as first assumed. Large intervals as in figure 4.13d has to change the sediment

parameters closer to silt than clay or mud, which might be an incorrect assumption when considering the environmental data, even though the values of this parameters are a bit uncertain.

The parameters t_{num} and t_{bet}, which are chosen for the best estimations gives a relative large number of values, but doesn't explore the length of the propagation very much. The step range correlates with the ship velocity where high values explores a large length of the propagation field, but isn't very in dept and visa versa. The time step of 1 isn't preferred which will result in similar problems as with low t_{num} and therefor it is preferred that when t_{bet} decreases the t_{num} should be increased.

Looking at large boundaries the sequence of areas with low loss are in a line across the parameter space like the noisy synthetic data, but with a higher slope and may be caused by the short horizontal range the ship is passing by at. The error of the estimations are fairly high, from 0.4130 and up, which is caused by the SNR and variance in the signal. This also causes some other parameters than the real parameters to be closely matched with the processed data.

The ASHS and ASDE search are represented in the figures 4.14 and 4.15 where a new estimation of the parameters is made at each iteration. The real parameter values are given in IV and the real value used for d_s is considered to be d_s which gives the best estimation of the parameters in the 2D search. The t_{num} and t_{bet} are 24 and 3 for this two cases shown here, with bottom properties c_s 1516 m/s and ρ_s 1520 kg/m^3. The error in the last figure is the calculated difference between the estimated parameter value and the real parameter value and are made to more closely see the difference between the estimated and real parameter error. Further exploration of the global search is given in appendix B.3.1.

This search seems to be fairly accurate and similar to the 2D search when the search interval is for small range such as 10 to 100 meters, see figure 4.14. The ship velocity is either 3.2 or 3.25 m/s and range is either 68 or 71 meters which are close to the assumed real values, but the d_s is jumping up and down and don't seem to have a constant value. This is because the d_s have more than one value, which combined with the other parameters gives almost the same error as the best estimation from the 2D search.

With a range interval of 10 to 500 meters the ASHS and ASDE has a chance of find the same solution as the 2D search. There are also solutions at 56 and 108 meters and 2.8 and 3.8 m/s for various source depths. This shows that a search over to large an interval is more uncertain when using the global algorithm than

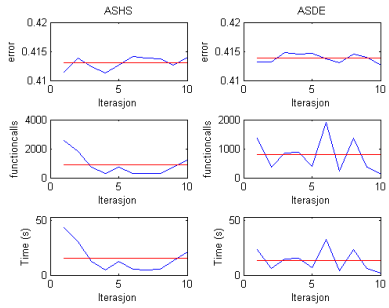

(a) Error, function calls and time used on estimation.

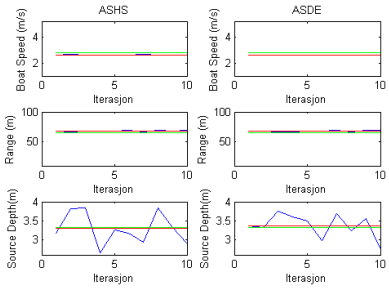

(b) Estimated parameters.

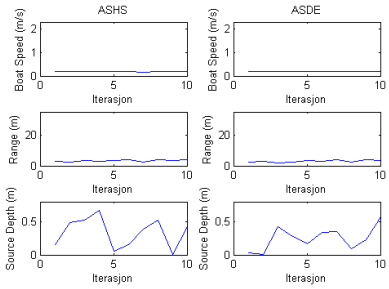

(c) Error of estimated parameters.

Figure 4.14: ASHS and ASDE search of Jumbo, the blue line is the estimated value, the red is the mean value of the estimates and the green line is the real value. The search is done 10 times with the same parameters as for figure 4.13a, the d_s are unknown and with average search intervals, see table XIII for the mean estimated parameters and the parameters used in the estimation.

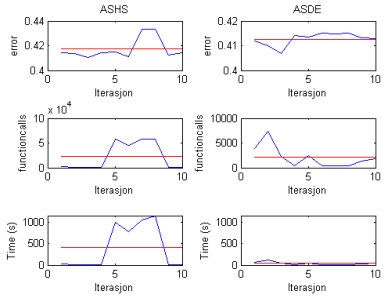

(a) Error, function calls and time used on estimation.

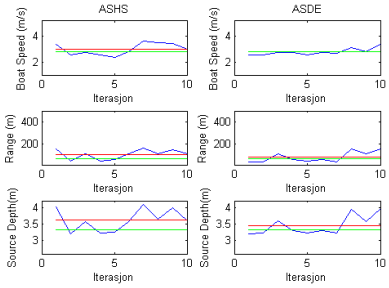

(b) Estimated parameters.

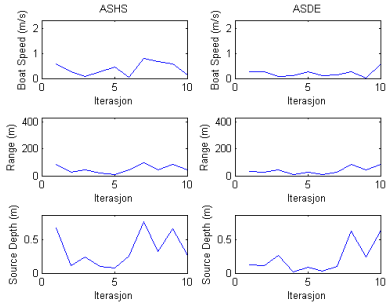

(c) Error of estimated parameters.

Figure 4.15: ASHS and ASDE search of Jumbo, the blue line is the estimated value, the red is the mean value of the estimates and the green line is the real value. The search is done 10 times with the same parameters as for figure 4.13a, the d_s are unknown and with large search intervals, see table XIII for the mean estimated parameters and the parameters used in the estimation.

the 2D search, which is caused by using more unknown parameters and the variance in the signal. The figures in 4.13 for the 2D search shows that there is a minimum at 56 meters and 2.7 m/s that the global search algorithm finds because both fulfill the stop criteria. The solution of 108 meter is caused by the source depth, which moves the area of low loss in the parameter space. With enough variance in the signal the error of least loss is so high that this point fulfill the stop criteria.

The ASHS and ASDE are operating a little differently, where the ASDE seems generally faster than the ASHS and finds more consistent parameters. This may be caused by how the different global algorithms work or the control parameters might not give the algorithms exactly the same searching properties.

4.5.2 Småen at Nilus-A

The 2D search of the recorded signal of Småen at NILUS-A is given in figures 4.16 with dB scale and the estimated parameters of the figures are given in table XIV. The figures presented is the best estimations which was found for the different combinations of parameters. Further exploration of the parameter space is shown in appendix B.3.2. The data is selected with a chosen number of t_{num} and t_{bet}, where 0 of the time blocks are after CPA and the rest are before. This was found to give the best estimation for the recording and the CPA is moved 2 time blocks after the calculated CPA to avoid the clipping.

The area of low loss for Småen stretches over a much larger area around the parameters found by AIS than for Jumbo. About 3.5 m/s up and down the velocity parameter and 30 meters in both direction of the horizontal range parameter, and there are at least 4 points that can be looked at as a possible solution. This creates a lot of uncertainty of which values are the best estimated. There is a also another large area around 16 m/s and 500 meter with low loss, which makes the estimation of the parameters more uncertain.

The figure 4.7b shows that the frequency values bellow 120 Hz might not represent the propagation field in a good way. The propagation field isn't as visible for this recording as for Jumbo. There are high SNR around 400 and some around 900 Hz which is important to select some values from these areas. The frequencies 138, 235, 343, 479, 680 and 878 Hz gives appropriate results and is used for all the results presented in this section and in the appendix B.3.2.

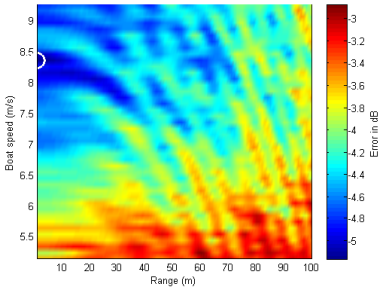

(a) Result with the expected set of parameters with a bit large time block spacing and small search intervals.

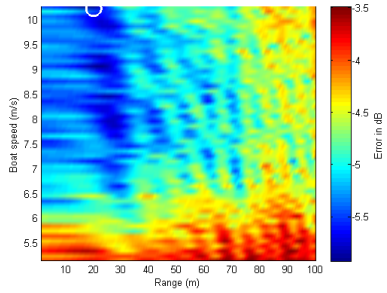

(b) Result with the expected set of parameters with small search intervals.

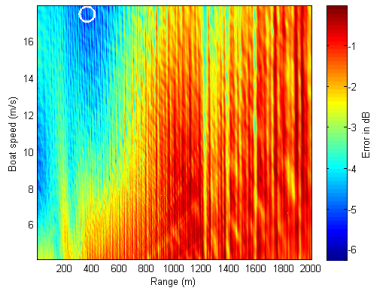

(c) Result with the expected set of parameters with a bit large time block spacing and large search intervals.

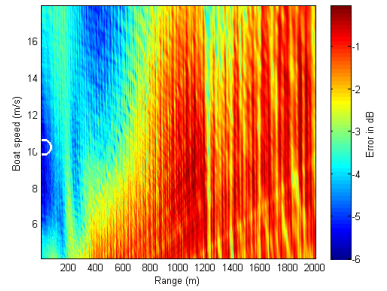

(d) Result with the expected set of parameters with large search intervals.

Figure 4.16: 2D search of Småen, plotting the cost function error at each combination of the parameters with log scale loss. The t_{num}, t_{bet}, d_s, c_s, ρ_s and the search intervals are searched for good results, see table XIV for the estimated parameters and parameters used in the estimation.

The source depth which is given in table IV isn't as close to the value that gives good estimations of the parameters as for the Jumbo case. The parameters t_{num} and t_{bet} that are chosen for the best estimations gives a relative large range and high number of time blocks, which stretch out to the -2 minutes mark, but doesn't go into details.

For the Småen case the c_s 1502 m/s and ρ_s 1500 kg/m^3 finds relative good estimations for range up to 2000 meters, as the figures in 4.16a and 4.16d shows. Figure 4.16d and figure 4.16a on the other hand shows that even closer

Table XIV: The estimated parameters of 2D search with error of Småen from the figures in 4.16, including the parameters to create them.

Figure	Estimated ship velocity (m/s)	Estimated hor. range (m)	Error	v_{si} (m/s)	d_{cpai} (m)	d_s (m)	t_{num}	t_{bet}	c_s (m/s)	ρ_s (kg/m^3)
4.16a	8.04	1.04	0.4882	5.1-10.3	1-100	1.4	24	6	1502	1500
4.16c	17.44	366	0.4857	5.1-18.0	1-2000	1.4	24	6	1502	1500
4.16b	10.22	20	0.5004	5.1-10.3	1-100	1.4	24	5	1502	1500
4.16d	10.22	20	0.5004	5.1-18.0	1-2000	1.4	24	5	1502	1500

Table XV: The mean estimated parameters from global algorithm search with error of Småen from the figures 4.17 and 4.18, including the boundary condition of the searched parameters and using the same properties as 4.16a. The mean estimated parameters from global algorithms with error, including the parameters to create them.

Figure	Global algorithm	Mean ship velocity (m/s)	Mean hor. range (m)	Mean source depth (m)	Error	v_{si} (m/s)	d_{cpai} (m)	d_{si} (m)	t_{bet}
4.17	ASHS	9.04	8	2.00	0.655	5.1-10.3	1-50	0.8-2.8	6
	ASDE	9.04	12	1.68	0.663	5.1-10.3	1-50	0.8-2.8	6
4.18	ASHS	10.2	22	1.83	0.4183	5.1-10.3	1-50	0.8-2.8	5
	ASDE	10.2	22	1.96	0.4135	5.1-10.3	1-50	0.8-2.8	5

estimation of the parameter at short range, but doesn't work for larger intervals. The 2D search finds some close parameter values at other values of c_s and ρ_s as shown in the appendix B.3.2.

The areas of good estimations in the parameter space for Småen seems to be larger than for the ones in Jumbo, this shows that the signal might consist of larger variance and low SNR. Another option is the distance at CPA is very close and the vessel is light with a low source depth, which has a flatter propagation field. This may be the reason for large area of low loss if it is combining this with lower SNR than Jumbo and some variance in the signal.

When looking at the search over larger intervals of range and velocity, the low loss line becomes more visible, but it's moved up in the parameter space compared with Jumbo and the synthetic data. This may be caused by the short d_{cpa}, because the transmission loss is low from this point to a fairly large range if the modeled propagation field in figure 4.19 can represent this case, which makes it more unique than d_{cpa} at longer range.

The ASHS and ASDE search of Småen are represented in the figures 4.17 and B.9. The parameter value that are assumed to be the real ones are given in IV and the real value of d_s is considered to be the calculated d_s, because the one used in the 2D search have such a large area with low loss. More results from the global algorithms are given in appendix B.3.1.

The global search finds some relative close estimation of the parameters when using c_s 1500 m/s and ρ_s 1502 kg/m^3 with t_{num} 24, t_{bet} 5 and t_{bet} 6 for small parameter intervals. The range estimation seems to be fairly close, but with a higher boat speed and a changing source depth and is caused by the large low loss area. Figures 4.16d and B.13b shows that the area with good estimations is around 1 to 20 meters in range and from 8 to 10 m/s for t_{bet} 6, but around 20 meters and 10 m/s for t_{bet} 5. This is a whole other matter for the average and large parameter interval where the horizontal range is estimated to be 100 meters and the ship velocity is 10 m/s. The 2D search seem to have a point at 10 m/s which has low loss and with different source depth there is apparently a range at 100 meters which has lower loss than shorter range, as shown in appendix B.3.2.

The ASHS and ASDE are for this case operating more or less similar and find more or less the same value. This may be caused by the fact that the search, which yielded good estimations for Småen, is done over smaller intervals of the parameters.

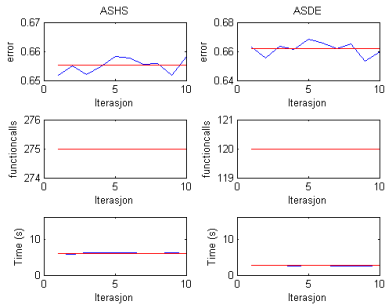

(a) Error, function calls and time used on estimation.

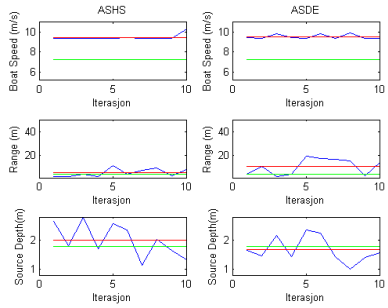

(b) Estimated parameters.

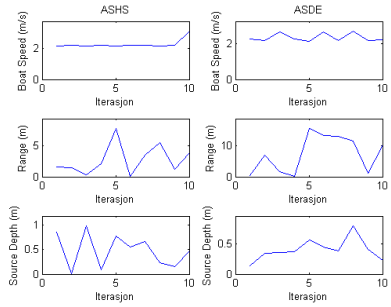

(c) Error of estimated parameters.

Figure 4.17: ASHS and ASDE search of Småen, the blue line is the estimated value, the red is the mean value of the estimates and the green line is the real value. The search is done 10 times with the same parameters as for figure 4.16a, the d_s are unknown and with small search intervals, see table XV for the mean estimated parameters and the parameters used in the estimation.

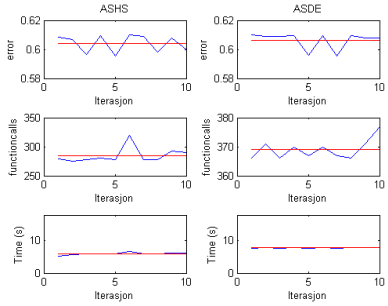

(a) Error, function calls and time used on estimation.

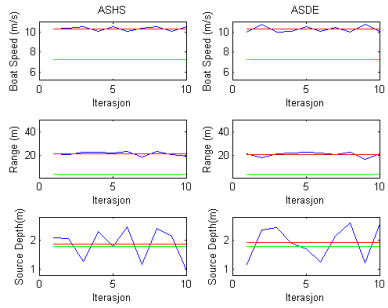

(b) Estimated parameters.

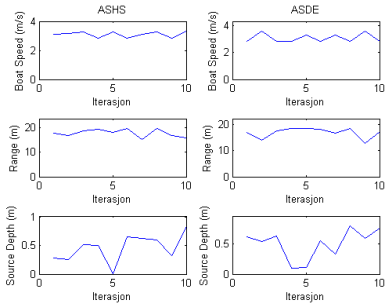

(c) Error of estimated parameters.

Figure 4.18: ASHS and ASDE search of Jumbo, the blue line is the estimated value, the red is the mean value of the estimates and the green line is the real value. The search is done 10 times with the same parameters as for figure 4.16b, the d_s are unknown and with small search intervals, see table XV for the mean estimated parameters and the parameters used in the estimation.

4.5.3 Summary of results

The best estimations of the parameters and its error are displayed in tables XVI and XVII.

Table XVI: Best estimated ship velocity with velocity error.

Recording	Ship velocity (m/s)	Estimated Ship velocity (m/s)	Ship velocity error (m/s)
Jumbo at NILUS-A	2.83	2.63	0.20
Småen at NILUS-A	7.20	8.04	0.84

Table XVII: Best estimated horizontal range at CPA with range error.

Recording	Horizontal range (m)	Estimated horizontal range (m)	Horizontal range error (m)
Jumbo at NILUS-A	65	69	4
Småen at NILUS-A	3.75	1.04	2.71

This parameters can be used to recreate the ship path of the boat, which are compared with the recorded AIS ship path in figure 4.19.

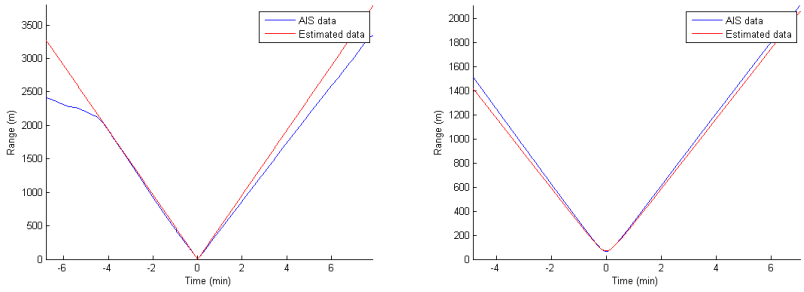

(a) Småen (b) Jumbo

Figure 4.19: The distance between the NILUS-A and the ship, where the blue line is the AIS recordings and the red is the estimated ship path.

This shows that the estimated ship paths is closely matched to the recorded ship paths close to the CPA, but starts to deviate at larger range.

4.5.4 Uncertainty

There are several factors contribute to uncertainty of the parameter estimation and is described here.

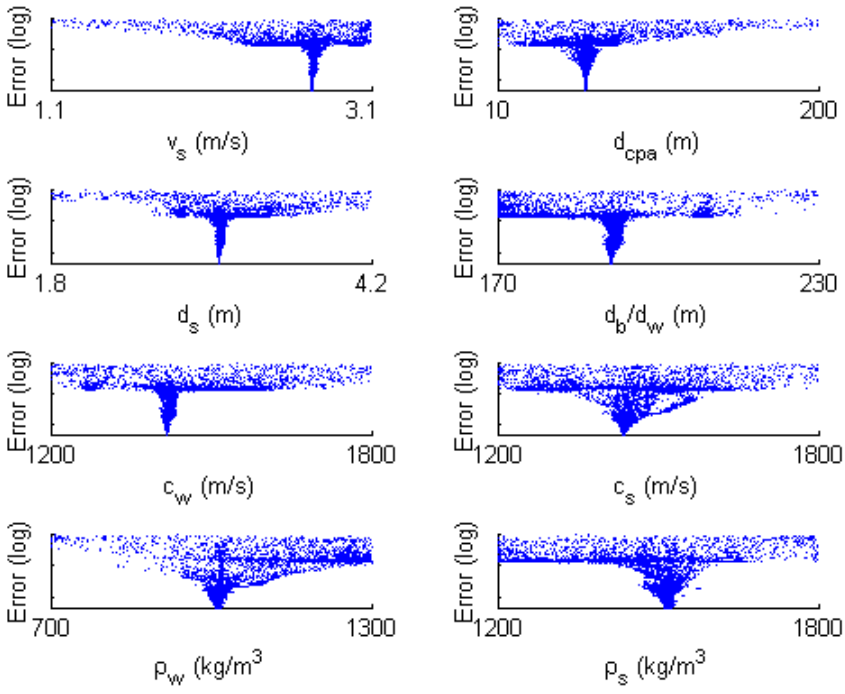

Figure 4.20: Cost function error in dB is plotted at each function call for each variables during a run of ASHS with stop criteria of 0.001. The plots gives an impression of each variables sensitivity.

The sensitivity analyses is given in figure 4.20, which gives an idea of which variables that have the largest impact on the cost function error. This analyzes is done by setting all the parameters shown in 4.20 as unknown and run the ASHS with a stop criteria of 0.001. It can be seen that some variables can have a more than on value and return low loss. This indicates that these variables are less sensitive and more difficult to estimate. These plots shows that the ship velocity and the source depth are most sensitive and d_{cpa} closely follows if very low loss is considered, but is more inaccurate at higher loss.

Another source of uncertainty is the sensors on the NILUS which has an accuracy of ±3 dB, which affects the amplitude which is recorded and the propagation field which is calculated from this signal.

Low SNR makes the propagation pattern less visible and the estimation will suffer from it, but it's hard to calculate in which extent this affects the estimation.

The signal processing will account for some loss of data where the welch estimation reduces the frequency resolution and the values is smoothed.

The GPS account for two different sources of uncertainties which are the NILUS-node location and the ship location. There is not given more data on how accurate the position of the boat is and is assumed to be ± 10 meters from [10]. The AIS data is also given from the antenna on the ship which is most likely near the cabin which usually is fairly close to the propeller. This gives an uncertain amount of error which will be of a few meters. The NILUS-node has an accuracy of around ±10 meters as well.

The source depth from the AIS data is calculated from the mean draft which will give some error when using this value. The depth is assumed to be around ±1 meters.

The receiver depth have an accuracy of ±3 meters as described in section 3.2.

The last source is the Lloyd mirror model which isn't a perfect reconstruction and is only accurate for short range. This gives a lot of uncertainty when t_{num} and t_{bet} are large and the interval of the parameters causes the model to search beyond it's accurate range.

Chapter 5

Discussion

This thesis has developed a method for estimating ship velocity and the horizontal range at CPA of a ship passing for ship tracking. FFI has deployed sensors to record ship passings outside Horten and this method has been used on two such recordings at a location. The method used are based on Willmut and Chapmans matched field inversion which are tested for an array of hydrophones and a the source is a sound projector, which generates continuous wave tones, see [18]. In this thesis the attention has been on reducing the variance of the noisy signal, make a suitable search algorithm and find sufficient results with the Lloyd mirror propagation model.

There where two data samples suitable for the matched field inversion method and some data in these recordings had problem with amplitude clipping, which made some data in the recording useless and lead to manually avoiding this data to prevent bad estimations. This combined with some variance in the signal after welch spectral estimation, made that both the time blocks and frequency values in the interval of 50 to 1000 Hz had to be manually chosen by analyzing the spectrum of the sample.

A reference for the estimation method to be compared with is necessary and the recorded AIS data are used, which have some uncertainty. Together with the uncertainty of the position of the sensor node the error of this recorded distance might be up to ±20 meters, which is high when considering the recorded distance for the Småen and Jumbo are 3.75 and 65 meters. This might also affect the assumption of constant velocity and straight ship path, but the recorded

samples doesn't give any visible sign of inconsistencies in the spectrum of the recordings, which makes this less probable. The recorded ships velocity are 7.20 and 2.83 m/s and these values have unknown uncertainty, but they are based on the path recorded by AIS and can be assumed to have an uncertainty related with the uncertainty of the recorded distances.

First the method is tested with noisy synthetic data, where the measured data is simulated with a noisy Lloyd mirror model. This estimations shows the limitations of the method and the affect it has on the loss over the parameter space. The observations that are made here are also made during the search for good estimations in the Jumbo and Småen data samples, but the cause can be more easily localized with ideal synthetic data. During these simulations it was discovered that the variance is a deciding factor in finding good estimation, because of how the cost function calculates the error. Thats why the limitation of the SNR is dependent on the magnitude of the variance and is difficult to predict, but with the figures presented in the results and the appendix, a limitation may be set at 5 dB when considering noise with variance. This is at the point of the limitation and should be higher when not considering ideal data, between 10 and 15 dB. The limitation of the number of time blocks in this simulations should at least be 12. This value is low and a higher number should be used, especially when there is no time limitation for the method.

The source depth is discovered to change the outcome of the estimation a lot, but varies a lot when using it as the third unknown in the global algorithms. The observations implies that the source depth is hard to estimate. The sensitivity estimation shows that the source depth is very sensitive and should be easy to estimate, which somewhat contradicts the observations. On the other hand, the error of the cost function is fairly high for the estimation and not nearly as low as 0.001 as in the sensitivity analyzes and may be the cause of this contradiction. That is why a good recording of this parameter is desired, but there is only recorded a mean draft for the ships involved. On the other hand the estimated source depth seem to be inside the uncertainty of the AIS data.

The recording of Jumbo at NILUS-A have a sufficient SNR such that the propagation pattern is visible. When using 2D search a suitable source depth is used and with average parameter interval and the bottom properties are considered to be clay, the area of low loss expands ± 15 meters and ± 0.75 m/s. This area of low loss can be looked at as a analytical approximation of the uncertainty of the estimation, where a possible solution may be found, like the two minimum points which is hard to distinguish as the global minimum. This two points is caused by

the fact that the recorded data doesn't give a perfect propagation pattern because of the lower SNR caused by ship traffic, some variance in the relevant frequency interval, not perfect calculated CPA and that the channel isn't ideal for the Lloyd mirror model, like flat sea floor bathymetry. The least loss parameters found are 2.63 m/s and 69 meters and are sufficiently good estimations of the real values if the estimations uncertainty is considered, which have lower uncertainty than the real values. When considering large intervals of the parameters the estimation finds the least loss values at very high parameter values and might be caused by the lack of accuracy of Lloyd mirror model at this range. This is only relevant when the boat distance is entirely unknown and not so much for this case. The global search algorithm yields this two points in the low loss area as solutions with various source depth, but there is found solution at lower loss with higher source depth at around 120 meters and 4 m/s, which isn't close to the real values and caused by not ideal propagation pattern. This makes the global search algorithm only reliable for search interval bellow 100 meters for the Jumbo case.

The recording of Småen at NILUS-A are much like Jumbo but with lower SNR, which cause less visible propagation pattern and it seems to be a little more variance in the signal too. When there is considered small parameter intervals and clay as the bottom properties, the area of low loss for the 2D search expands ±30 meters and ±3.5 m/s with at least 4 points that can be the global solution and is most likely caused by the same things as for Jumbo. The least loss parameters found are 8.04 m/s and 1.04 meters and are close to the real parameter value, but if the uncertainty of the estimation is considering it will be questionable good because it has more uncertainty than the real values. When considering large intervals of the parameters the estimation finds the least loss at higher parameters like Jumbo, mots likely because of Lloyd mirror. When using the global search algorithm the best values found are about 10 m/s, but with shifting source depth and distance at CPA, which variates between about 1 to 20 meters. This is for a small search intervals, but it finds better estimation about at about 100 meters when considering larger and makes the global algorithm not reliable for the Småen case when considering larger parameter intervals.

The global search algorithms for both Jumbo and Småen shows some resemblance to a local search algorithm, because they seem to choses one of the first local minimum they find in the parameter space. This can be caused by the high loss in the parameter space, which makes it hard to chose a stop criteria to fit the search for the estimation. Another possibility is that the SNR and variance may be low/high enough for the method to consider other parameters than the real ones as equally good. The control parameters in the two global algorithms may

also be as appropriate as first thought, this might make the algorithm more like a local optimization algorithm. On the other hand, when considering estimation for larger parameter intervals with more than one area of low loss it still finds the area with least loss, so it may only be a problem with to stop criteria.

The ship tracking seems to be quite close to the AIS ship tracking, even over fairly large range. The ship velocity is the accuracy over large range from CPA and the d_{cpa} is of course the accuracy at the CPA, which makes the uncertainty and the evaluation of result of the tracking directly connected with the estimation of the parameters.

Suggestions for future research and improvement of this method are

- Use the estimation method on more real data to find further study the methods limitations.
- Resolve the problem with the clipping such that the whole data set might be used in the matching inversion method and such that the propagation field don't have to be analyzed manually before using the method.
- Low SNR makes the propagation pattern less visible and the method will suffer in accuracy from this and testing the NILUS-node at an area with less traffic might improve the SNR.
- Reduce the variance further such that the propagation pattern is less variating.
- An improvement of the Lloyd mirror model might make estimations at larger range more accurate.
- The source depth proved to be an important factor and a better estimation of this would be preferred, the estimation may profit on more detailed bottom properties as well.

Chapter 6

Conclusion

In this thesis a matched field inversion method has been developed to estimate the horizontal range at CPA and ship velocity for tracking purposes using Lloyd mirror propagation model. The measured data is recorded and processed ship noise at a single hydrophone.

The estimation was performed on two time sample, which was provided by FFI. The results points to some suggestions on what the estimation requires:

- The recorded data should have high enough SNR so the propagation pattern is visible.
- The variance in the recording signal should be sufficiently reduced.
- A good estimation of the source depth should be acquired.
- The 2D search method should be used when the unknown parameters have larger boundaries.
- ASHS and ASDE should be faster and can be applied when presented with a problem with small parameter boundaries and sufficiently high SNR.
- A sufficient amount of data should be used in the estimation, such as 6 frequencies spread over the relevant frequencies (suggested 50 - 1000 Hz) for 24 time blocks spread periodically over the ship path.
- The search of good estimations shouldn't exceed the limitations of the propagation model (suggested horizontal range limit of Lloyd mirror is 300 meter and flat bathymetry).

This method makes it possible to estimate the horizontal range and ship velocity with some error at sufficiently small range and velocity, provided that most of the suggestions are fulfilled, which makes it possible to track a ship. The method may help establishing a routine that is suited for a easily deployable system such as NILUS.

Bibliography

[1] Iyad Tumar Anuj Sehgal and Jürgen Schönwälder. Effects of climate change and anthropogenic ocean acidification on underwater acoustic communications. *IEEE Journal of Oceanic Enginering*.

[2] SAIV AS. Ctd/std - model sd204 (ctd profiler).

[3] L.M. Brekhovskikh and Yu.P. Lysanov. *Fundamentals of Ocean Acoustics*. Springer.

[4] David C. Calvo. *Quick Introduction to Using The Naval Reserch Lab's RAM Parabolic Equation (PE) Code That Includes Bottom Loss*. Naval Research Laboratory.

[5] William M. Carey and Richard B. Evans. *Ocean Ambient Noise*. Springer.

[6] Michael D. Collins. *User's Guide for RAM version 1.0 and 1.0p*. Naval Research Laboratory.

[7] Stian Coward. A method for remtoe sensing of acoustic ship noise. Master's thesis, Norwegian University of Science and Technology.

[8] Ultra Electronics. An/ssq 53d(3) directional passive sonobuoy.

[9] A. Rüdiger G. Heinzel and R. Schilling. Spectrum and spectral density estimation by the discrete fourier transform (dft), including a comprehensive list of window functions and some new at-top windows. Technical report, Max-Planck-Institut für Gravitationsphysik (Albert-Einstein-Institut), Teilinstitut Hannover.

[10] Officel U.S Government. Information about the global positioning system and related.

[11] Saeed Mosayyebpour Hannan Lohrasbipeydeh and T. Aaron Gulliver. Single hydrophobe passive acoustic sperm whale range and depth estimation. *IEEE Journal of Oceanic Enginering*.

[12] Jens M. Hovem. *Marine Acoustics*. Peninsula Publishing.

[13] Høgskolen i Ålesund. Matlab toolbox for ais messages, version 1.2.

[14] Finn B. Jensen and William A. Kuperman. *Computational Ocean Acoustics*. Springer.

[15] Kartverket. Sjøkart.

[16] Megan F. McKenna. Underwater radiated noise from modern commercial ships. *Acoustical Society of America*, 131(1):92–103, January 2012.

[17] Stan E. Dosso Michael G. Morley and N. Ross Chapman. Array element localization using ship noise. *Journal of the Acoustical Society of America*, 125(3):1403–1409, March 2009.

[18] N. Ross Chapman Michael J. Wilmut. Inversion of lloyd mirror field for determining a source's track. *IEEE Journal of Oceanic Enginering*, 32(4):940–947, October 2007.

[19] John G. Proakis and Dimitris G. Manolakis. *Digital signal processing*. Prentice Hall.

[20] Connie E. Solberg Roald Otnes and Paul van Walree. Ffi - fokus: Kommunikasjon og nettverk under vann). Technical report, Norwegian Defence Research Establishment (FFI).

[21] Urmila Dattaa Vidar Forsmoa Jon Kjølla Torbjørn Nordfjellmarka Stine K Richardsena Roald Otnesa, Helge Buena and Paul van Walree. Experiences from using the demonstrator system nilus (networked intelligent underwater sensors). Technical report, Norwegian Defence Research Establishment (FFI).

[22] Cherry Wakayama Rockie Ricks, Doug Grimmett. Passive acoustic tracking for cueing a multistatic active acoustic tracking system. Technical report, Maritime Systems Division.

[23] Niklas Saxlund Skyberg. Study of optimization algorithms for underwater acoustic applications. Master's thesis, Norwegian University of Science and Technology.

[24] Rainer Storn and Kenneth Price. Differential evolution a simple and efficient heuristic for global optimization over continuous spaces. *Journal of Global Optimization*, 11.

[25] International Telecommunication Union. Technical characteristics for an automatic identification system using time-division multiple access in the vhf maritime mobile band.

[26] Geem Z. W. *Music-Inspired Harmony Search Algorithms*. Springer.

[27] Stephen C. Wales and Richard M. Heitmeyer. An ensemble source spectra model for merchant ship radiated noise. *Acoustical Society of America*, 111 (3):1211–1231, March 2002.

[28] Michael J. Willmut and Stan E. Dosso. Data uncertainty estimation in matched-field geoacoustic inversion. *IEEE Journal of Oceanic Enginering*, 31(2):470–479, April 2006.

[29] Lurton Xavier. *An Introduction to Underwater Acoustics*, chapter 2. Springer.

Appendix A

RAM

There are two propagation models which are used: Lloyd mirror model and RAM (Range dependent acoustical model). The Lloyd mirror is described in detail in the theory chapter 2 and the RAM model is partly described here and in more details in the project.

The RAM is a numerical solution of the parabolic equation method, based on the split-step Padè solution and is an efficient method according to [6]. It handles range dependent environments as a sequence of segments of range independent environments, such as sound speed and Bathymetry.

The RAM is coded in FORTRAN in comparison with the rest of the code which is coded in MATLAB. The Bathymetry is interpolated in range in the RAM code to the current range step. All the input files are stored in an text file before it is set into the RAM code. This inputs have to be selected properly and a guide has been provided by FFI [4], where a ratio between the parameters are suggested to ensure good results and it is possible to do a convergence test to see if it obtains proper values.

Table XVIII: Control parameters in RAM.

dr	1.0	ndr	10
dz	0.25	ndz	4
$zmplt$	100.0	np	5
ns	1	rs	0.0

The RAM code returns the transmission loss and to find the amplitude value of

the RAM the calculations has to by inversed. The control parameters in the RAM code are given in table XVIII. Where dr is the range steps, ndr range output steps, dz is the depth steps, ndz depth output steps, $zmplt$ is the vertical extent of the domain to output, np is Pade terms, ns is stability constraints and rs is radius of stability constraint.

The FORTRAN code of the RAM returns the propagation field with a range step of dr up to a given maximum range, $rmax$, and a new field has to be created for each frequency desired. If the RAM was to be used in the parameter estimation some problems would arise. Storing new values in a file for each new parameter that is explored and creating a propagation field from 0 to $rmax$ is very time consuming and the MATLAB script will crash because of memory usage when storing new data in the file. The main propagation model which is desired to be explored in this thesis is the Lloyd mirror, so an easy solution can been made by just creating a large propagation field matrix with maximum possible range of the parameter interval for each desired frequency. The values are picked from this matrix rather than creating a new field for each parameter, this is time consuming and will limit the range resolution, but will not crash the script.

Appendix B

Results

In this appendix, more results has been added for more information to analyze. The results in this chapter shows further how the method behaves for the different parameters.

B.1 Received data

The signal recorded over time are shown in figures B.1a and B.1b.

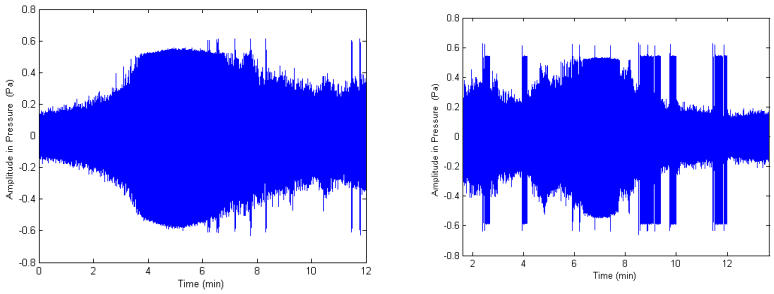

(a) Jumbo.

(b) Småen.

Figure B.1: The recorded time signal for Jumbo and Småen at NILUS-A.

For Jumbo the the amplitude of the signal is higher after the CPA than before which is caused by the propagation effects. For Småen the amplitude of the sig-

nal is a bit high around 2 minutes mark as discussed in section 4.3 and there is a lot of amplitude clipping in the signal.

B.2 Synthetic simulation

Further testing of the t_{num}, SNR and variance of the noise with 2D search and the global algorithms with the parameters in table VII.

Table XIX: The estimated parameters of 2D search with noisy synthetic data from figures in B.2 and B.3.

Figure	Estimated ship velocity (m/s)	Estimated hor. range (m)	t_{num}	SNR (dB)	variance
B.2a	5.12	250	24	0	0.5
B.2b	5.32	250	24	0	1.0
B.2c	5.13	251	24	-5	0.5
B.2d	5.12	251	24	-100	0.0
B.3a	5.12	250	10	10	0.5
B.3b	5.12	250	10	10	1.0
B.3c	4.03	131	8	10	0.5
B.3d	5.12	250	8	10	0.1

Table XX: The mean estimated parameters from global algorithms for noisy synthetic data from the figures B.5 and B.6.

Figure	Global algorithm	Mean ship velocity (m/s)	Mean hor. range (m)	t_{num}	SNR (dB)	variance
B.5	ASHS	5.27	260	12	-5	0.3
	ASDE	5.16	256	12	-5	0.3
B.6	ASHS	5.13	264	8	10	0.3
	ASDE	5.23	259	8	10	0.3

In figure B.2 the SNR and variance is changed and gives more or less good results when the magnitude of the variance is small, which further show what was discovered in section 4.4.

The figures in B.3 is made with 10 dB and different t_{num} and variance the figures shows further that low number of t_{num} starts to make the low error pattern for low velocity.

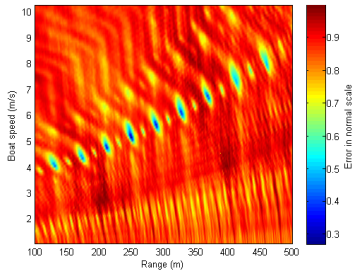

(a) Result of low SNR and average variance.

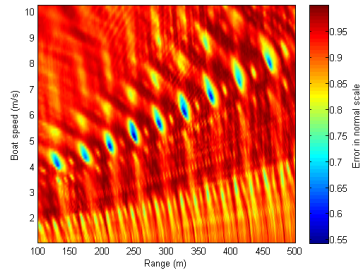

(b) Result of low SNR and high variance.

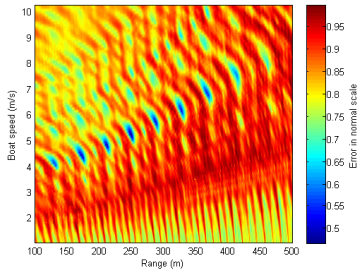

(c) Result of very low SNR and average variance.

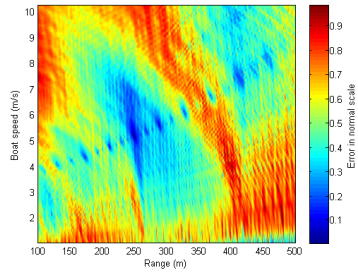

(d) Result where the noise is dominant and no variance.

Figure B.2: Further2D search of synthetic data, plotting the cost function error at each combination of the parameters with normal scaled loss. The SNR and variance of the noise are changed between each figure with t_{num} 24, where a SNR of 10 dB is considered on the edge of good SNR, see table XIX for the estimated parameters and the noise used in the estimation.

Further testing of the global algorithms is made to punctuate what was found in section 4.4.

The error and parameter of the ASHS and ASDE results in 4.4 is given here in figures B.4. The figures shows that the error variates with the magnitude of the variance and the time used on finding a good estimation increases because either of the cases mentioned in section 4.4.

The figures B.5 and B.6 show more testing with different t_{num}. These plots shows further that a signal with variance makes the global search algorithms find more than one good estimation of the parameters. Low number of time blocks also makes the global search algorithm finding other parameters than the correct

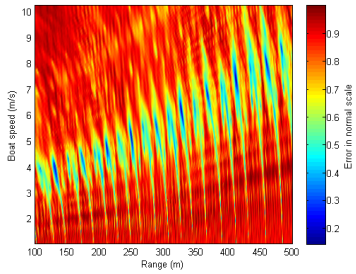

(a) Result of low t_{num} and average variance.

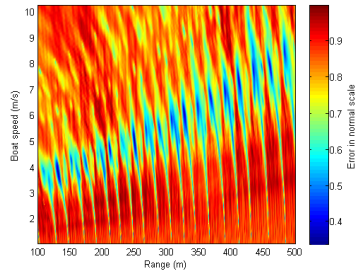

(b) Result of low t_{num} and high variance.

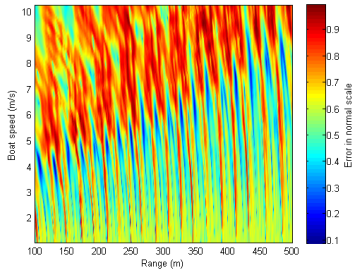

(c) Result of very low t_{num} and average variance.

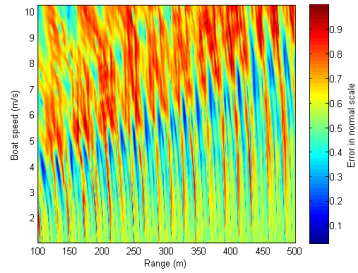

(d) Result of very low t_{num} and low variance.

Figure B.3: Further 2D search of synthetic data, plotting the cost function error at each combination of the parameters with normal scaled loss. The t_{num} and variance of the noise are changed between each figure with SNR 10 dB, where a t_{num} of 16 is considered on the edge of enough data, see table IX for the estimated parameters, noise and parameter used in the estimation.

ones. This is discussed in section 4.4.

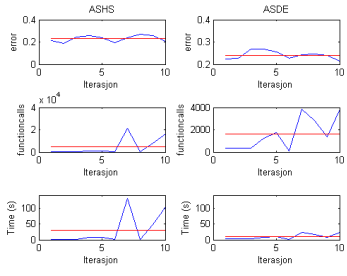

(a) Error, function calls and time used on estimation for 4.12a.

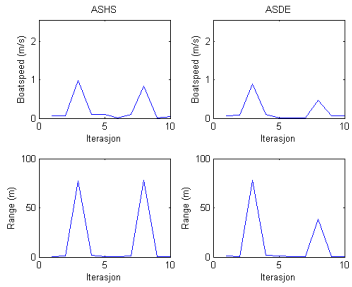

(b) Error of estimated parameters for 4.12a.

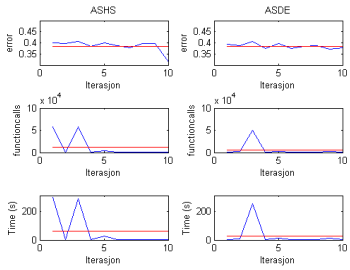

(c) Error, function calls and time used on estimation for 4.12b.

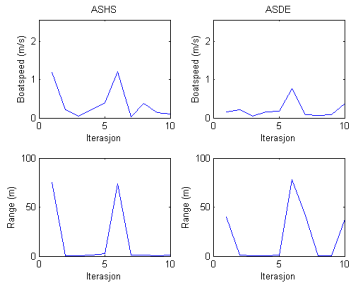

(d) Error of estimated parameters for 4.12b.

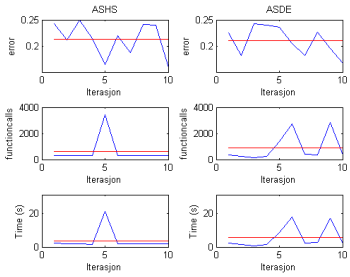

(e) Error, function calls and time used on estimation for 4.12c.

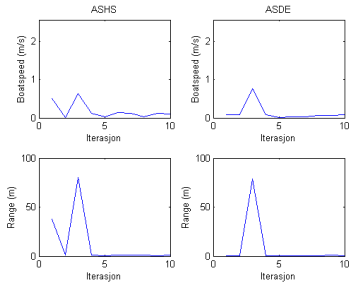

(f) Error of estimated parameters for 4.12c.

Figure B.4: Cost function error, number of function calls, time used and the error of the parameters when searching with ASHS and ASDE for noisy synthetic data of the cases in figure 4.12.

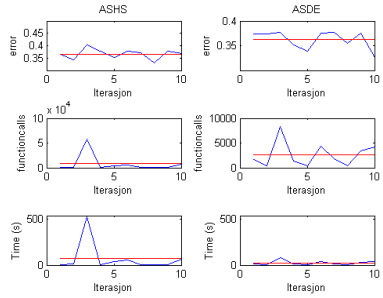

(a) Error, function calls and time used on estimation.

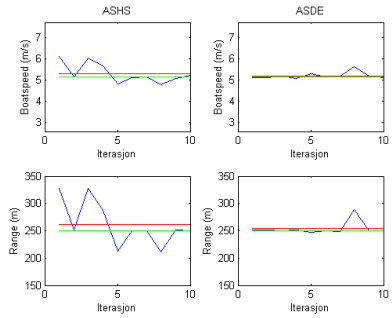

(b) Estimated parameters.

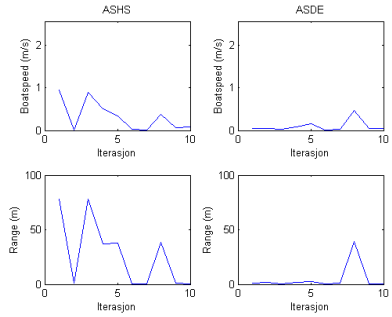

(c) Error of estimated parameters.

Figure B.5: ASHS and ASDE search of synthetic data, the blue line is the estimated value, the red is the mean value of the estimates and the green line is the real value. The search is done 10 times with average t_{num}, very low SNR and low variance, see table XX for the mean estimated parameters and the parameters used in the estimation.

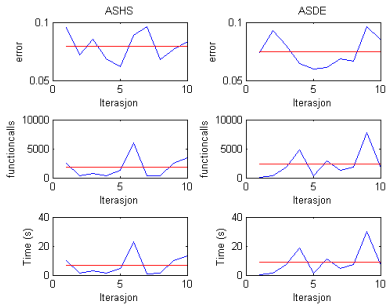

(a) Error, function calls and time used on estimation.

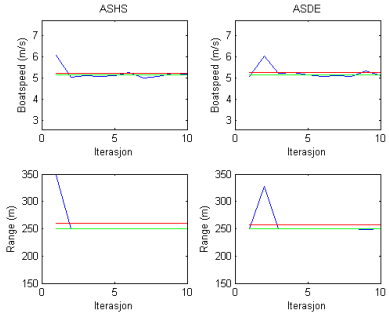

(b) Estimated parameters.

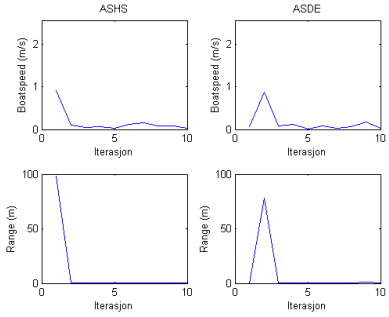

(c) Error of estimated parameters.

Figure B.6: ASHS and ASDE search of synthetic data, the blue line is the estimated value, the red is the mean value of the estimates and the green line is the real value. The search is done 10 times with low t_{num}, good SNR and low variance, see table XX for the mean estimated parameters and the parameters used in the estimation.

B.3 Estimation of recorded data

B.3.1 Jumbo at NILUS-A

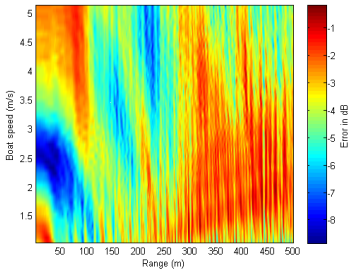

(a) Result with low number of time blocks, higher time block spacing, a bit high bottom properties and medium search intervals.

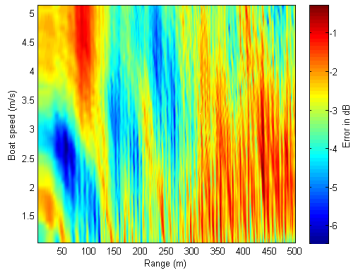

(b) Result with a bit low number of time blocks, a bit high bottom properties and medium search intervals.

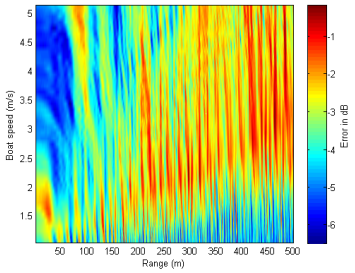

(c) Result with low number of time blocks, a bit high bottom properties and medium search intervals.

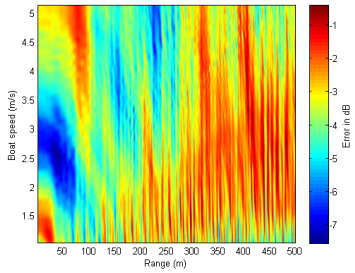

(d) Result with almost the expected parameters, apart from a bit high bottom properties, low source depth and medium search intervals.

Figure B.7: Further 2D search of Jumbo, plotting the cost function error at each combination of the parameters with log scale loss. The t_{num}, t_{bet}, d_s, c_s, ρ_s and the search intervals are searched for good results, see table XXI for the estimated parameters and parameters used in the estimation.

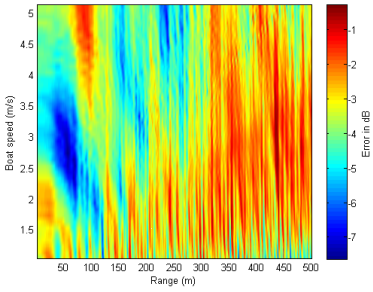

(a) Result with almost the expected parameters, apart from a bit high bottom properties, lower source depth and medium search intervals.

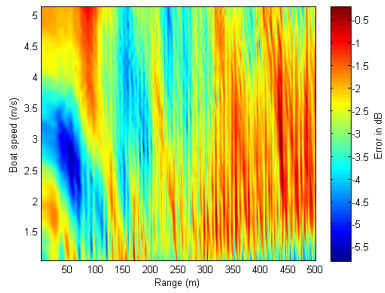

(b) Result with high number of time blocks, low time block spacing and medium search intervals.

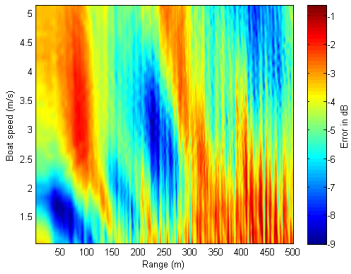

(c) Result with higher time block spacing, a bit high bottom properties, low source depth and medium search intervals.

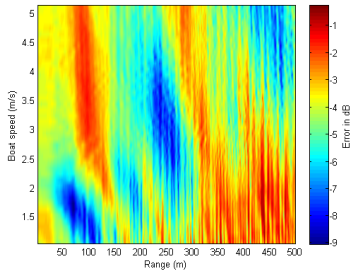

(d) Result with higher time block spacing, a bit high bottom properties, lower source depth and medium search intervals.

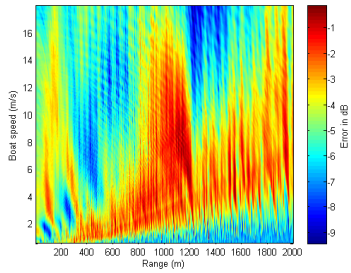

(e) Result with almost the expected parameters, apart from higher time block spacing and large search intervals.

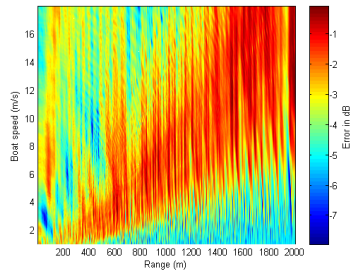

(f) Result with higher time block spacing, high bottom properties and large search intervals.

Figure B.8: Further 2D search of Jumbo, plotting the cost function error at each combination of the parameters with log scale loss. The t_{num}, t_{bet}, d_s, c_s, ρ_s and the search intervals are searched for good results, see table XXI for the estimated parameters and parameters used in the estimation.

The figures in B.7 and B.8 shows further display of the 2D search algorithm for Jumbo, log error for each combination of parameters. With results and properties in table XXI. There are some new observations in this figures which hasn't been mentioned before and that is that the pattern for few time blocks is visible for the simulation over large range. With some combination, as the figure B.8f shows, gives best solution at low velocity but at large range and the reasoning behind this is the same as for low number of time blocks. This might cause problem for the model if a ship passes by at longer range.

The figures shows how the search for the best estimation of the parameter value was done. There are many solution of the problem which are close to real parameter value. The the number of time blocks and time block spacing adjusted slightly until they converge on the best estimations, which is shown in this figures. Increasing the number of time blocks and spacing meets the problem of low SNR at large range. The recorded data don't seem to have continuously high SNR and no variance which causes that some combination of the t_{num} and t_{bet} more favorable than others.

The source depth affect of the source depth on the estimation becomes very visible when looking at this figures. A lot of the figures are simulated with larger sediment properties to see the affect of this parameters, which are relative little. The properties of the sediment may have more affect on the estimation if the recorded ship was at larger range.

The global algorithms in figures B.9, B.10 and B.11 uses c_s 1502 m/s and ρ_s 1500 kg/m^3. For larger intervals of the parameters the estimation is close, but variating and as figure B.11 shows, the search is random and might find estimates with low enough loss for the stop criteria to be triggered and unfortunately this is repeatedly the case in this figure.

Table XXI: The estimated parameters of 2D search with error of Jumbo from the figures in B.7 and B.8, including the parameters to create them.

Figure	Estimated ship velocity (m/s)	Estimated hor. range (m)	Error	v_{si} (m/s)	d_{cpai} (m)	d_s (m)	t_{num}	t_{bet}	c_s (m/s)	ρ_s (kg/m^3)
B.7a	2.34	33	0.3600	1.0-5.1	10-500	3.2	16	5	1540	1600
B.7b	2.73	57	0.4748	1.0-5.1	10-500	3.3	20	4	1540	1600
B.7c	3.43	68	0.4736	1.0-5.1	10-500	3.2	16	3	1540	1600
B.7d	2.53	39	0.4184	1.0-5.1	10-500	3.2	24	3	1540	1600
B.8a	2.70	57	0.4748	1.0-5.1	10-500	3.3	24	3	1540	1600
B.8b	2.73	57	0.5118	1.0-5.1	10-500	3.3	32	2	1516	1520
B.8c	3.10	227	0.3549	1.0-5.1	10-500	3.2	24	5	1540	1600
B.8d	1.73	70	0.3552	1.0-5.1	10-500	3.3	24	5	1516	1520
B.8e	16.90	1220	0.4130	1.0-18.0	10-2000	3.325	24	5	1520	1535
B.8f	5.03	1995	0.4093	1.0-18.0	10-2000	3.325	24	5	1575	1700

Table XXII: The mean estimated parameters from global algorithms with error of Jumbo from B.9, B.10 and B.11, including the parameters to create them.

Figure	Global algorithm	Mean ship velocity (m/s)	Mean hor. range (m)	Mean source depth (m)	Error	v_{si} (m/s)	d_{cpai} (m)	d_{si} (m)
B.9	ASHS	2.63	69	3.25	0.4113	1.0-5.1	10-100	2.6-3.8
	ASDE	2.63	69	3.28	0.4113	1.0-5.1	10-100	2.6-3.8
B.10	ASHS	3.15	118	3.25	0.4118	1.0-5.1	10-500	2.6-3.8
	ASDE	2.70	100	3.325	0.4113	1.0-5.1	10-500	2.6-3.8
B.11	ASHS	3.93	138	3.20	0.4191	1.0-5.1	10-500	2.6-4.3
	ASDE	4.30	163	2.76	0.4111	1.0-5.1	10-500	2.6-4.3

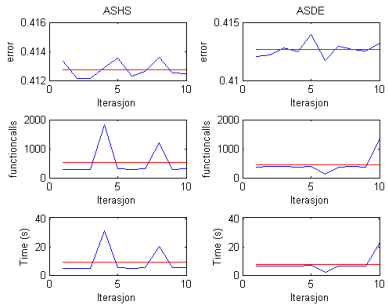

(a) Error, function calls and time used on estimation.

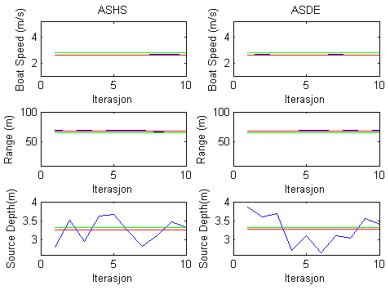

(b) Estimated parameters.

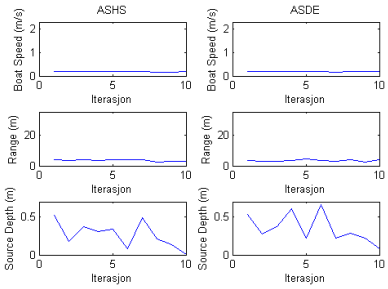

(c) Error of estimated parameters.

Figure B.9: Further ASHS and ASDE search of Jumbo, the blue line is the estimated value, the red is the mean value of the estimates and the green line is the real value. The search is done 10 times with the same parameters as for figure 4.13a, the d_s are unknown and with average search intervals, see table XXII for the mean estimated parameters and the parameters used in the estimation.

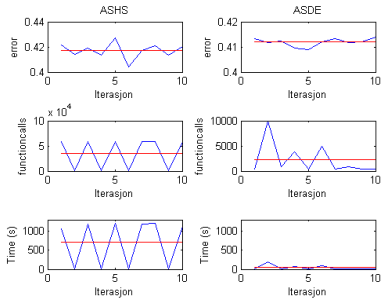

(a) Error, function calls and time used on estimation.

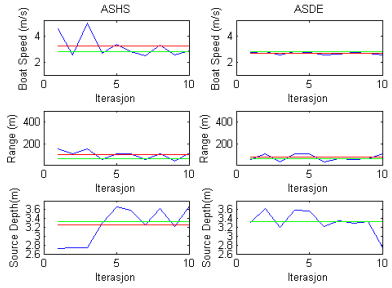

(b) Estimated parameters.

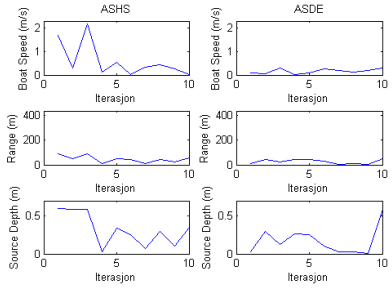

(c) Error of estimated parameters.

Figure B.10: Further ASHS and ASDE search of Jumbo, the blue line is the estimated value, the red is the mean value of the estimates and the green line is the real value. The search is done 10 times with the same parameters as for figure 4.13a, the d_s are unknown and with large search intervals, see table XXII for the mean estimated parameters and the parameters used in the estimation.

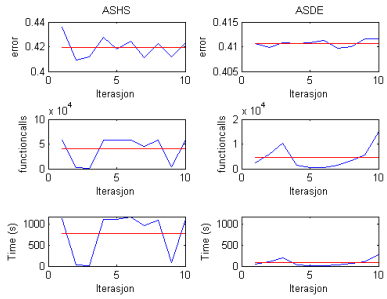

(a) Error, function calls and time used on estimation.

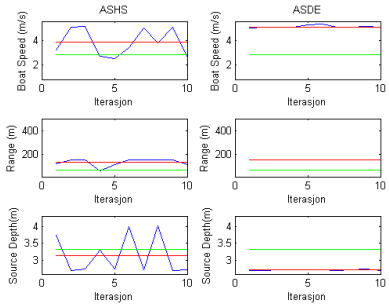

(b) Estimated parameters.

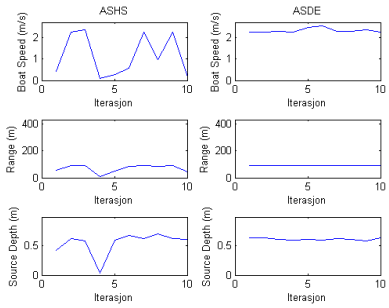

(c) Error of estimated parameters.

Figure B.11: Further ASHS and ASDE search of Jumbo, the blue line is the estimated value, the red is the mean value of the estimates and the green line is the real value. The search is done 10 times with the same parameters as for figure 4.13a, the d_s are unknown and with large search intervals and a bit larger ship velocity interval, see table XXII for the mean estimated parameters and the parameters used in the estimation.

B.3.2 Småen at NILUS-A

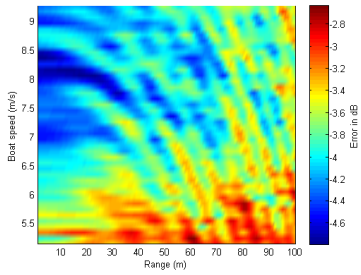

(a) Result with a bit high bottom properties and low search intervals.

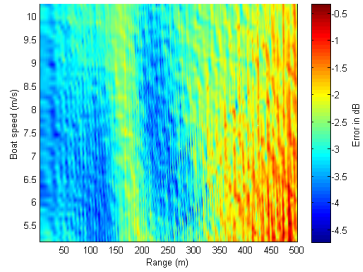

(b) Result with a bit high bottom properties, low source depth and average search intervals.

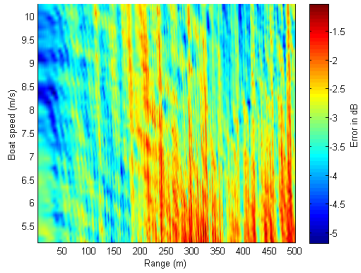

(c) Result with high bottom properties, high source depth and average search intervals.

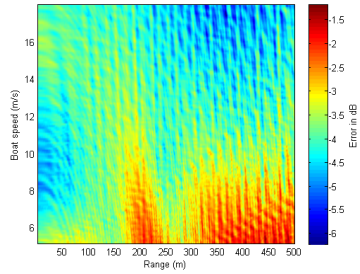

(d) Result with the expected set of parameters with a bit large time block spacing and average search intervals.

Figure B.12: Further 2D search of Småen, plotting the cost function error at each combination of the parameters with log scale loss. The t_{num}, t_{bet}, d_s, c_s, ρ_s and the search intervals are searched for good results, see table XXIII for the estimated parameters and parameters used in the estimation.

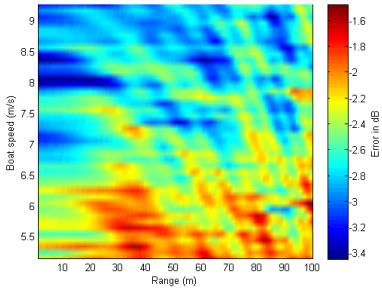

(a) Result with large number of time blocks, a bit large time block spacing, high bottom properties and small search intervals.

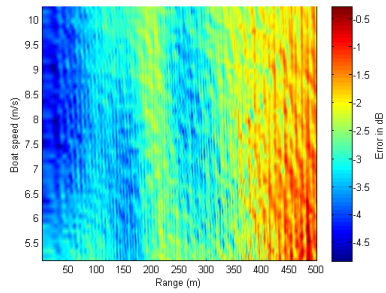

(b) Result with higher source depth, a bit high bottom properties and average search intervals.

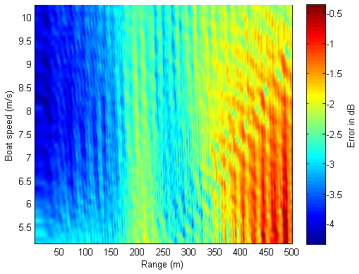

(c) Result with large number of time blocks, higher source depth, a bit high bottom properties and average search intervals.

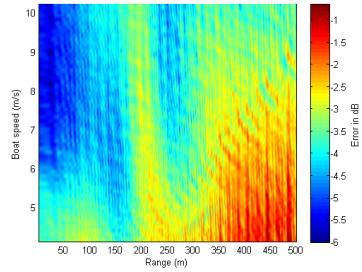

(d) Result with the expected set of parameters with average search interval.

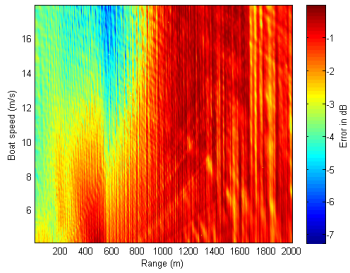

(e) Result with the expected set of parameters with a bit large time block spacing, high bottom properties and large search interval.

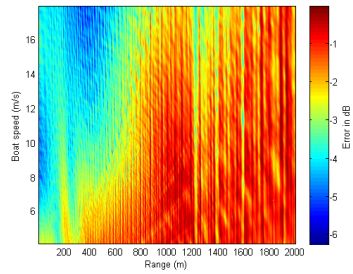

(f) Result with the expected set of parameters with a bit large time block spacing and large search interval.

Figure B.13: Further 2D search of Småen, plotting the cost function error at each combination of the parameters with log scale loss. The t_{num}, t_{bet}, d_s, c_s, ρ_s and the search intervals are searched for good results, see table XXIII for the estimated parameters and parameters used in the estimation.

The figures in B.12 and B.13 shows further display of the 2D search algorithm for Småen in log scale for each combination of parameters with results and properties in table XXIII. These figures shows some of the process on how the best estimations are found, where there are very large areas with low loss with some minimum points in them which makes the whole search difficult and its accuracy questionably. The best estimation seems to be figure B.12c when considering the error and the area of low loss, but to achieve this the sediment properties has to be change to silt which doesn't match with the predicted sediment. There are also some very low loss points at larger range for this estimation which makes it less good.

Figure B.13a shows that a higher number of time blocks used gives worse error as discussed in section 4.4. This error may also occur because the search stretches to the 3 min mark which is close to the other visible ship passing and gets an area with a lot of clippings, which are avoided.

Figure B.12a and B.13a doesn't manage to show how large the area with low loss is and is better shown with other figures, where the error is quite high for all figures and might make the plot show high error as good estimations as shown in figure B.13c, but is a bit contradicted by figureB.13b. This makes the simulation a bit misleading and the figure may not be as appropriate for displaying the estimation as first though.

The global algorithms in figures B.14, B.15, B.16 and B.17 uses c_s 1502 m/s and ρ_s 1500 kg/m^3. These figures further shows that the intended best estimation of the parameters isn't the globally best when considering different source depth. The t_{bet} 6 and t_{bet} 5 cases seems to behave very much alike at larger search intervals when ASHS and ASDE is used.

Table XXIII: The estimated parameters of 2D search with error of Småen from the figures in B.12 and B.13, including the parameters to create them.

Figure	Estimated ship velocity (m/s)	Estimated hor. range (m)	Error	v_{si} (m/s)	d_{cpai} (m)	d_s (m)	t_{num}	t_{bet}	c_s (m/s)	ρ_s (kg/m^3)
B.12a	8.04	21	0.5757	5.1-9.3	1-100	1.40	24	6	1540	1580
B.12b	6.74	256	0.5802	5.1-10.3	1-500	1.34	24	5	1580	1600
B.12c	8.34	33	0.3552	5.1-10.3	1-500	1.44	24	5	1575	1700
B.12d	17.44	366	0.4130	5.1-10.3	1-500	1.40	24	6	1502	1500
B.13a	8.04	1.04	0.6722	5.1-9.3	1-100	1.40	30	6	1575	1700
B.13b	7.84	30	0.6067	5.1-10.3	1-500	1.42	24	5	1540	1580
B.13c	7.84	30	0.6067	5.1-10.3	1-500	1.42	30	5	1540	1600
B.13d	10.2	33	0.5004	5.1-10.3	1-500	1.40	24	5	1502	1500
B.13e	17.44	366	0.4380	5.1-18.0	1-2000	1.40	24	6	1575	1700
B.13f	17.44	366	0.4857	5.1-18.0	1-2000	1.40	24	6	1502	1500

Table XXIV: The mean estimated parameters from global algorithms with error of småen from the figures B.14, B.15, B.16 and B.17, including the parameters to create them.

Figure	Global algorithm	Mean ship velocity (m/s)	Mean hor. range (m)	Mean source depth (m)	Error	v_{si} (m/s)	d_{cpai} (m)	d_{si} (m)	t_{bet}
B.14	ASHS	10.04	97	2.10	0.6119	5.1-10.3	1-100	0.8-2.8	6
	ASDE	10.00	93	1.63	0.6312	5.1-10.3	1-100	0.8-2.8	6
B.15	ASHS	13.14	121	1.72	0.5253	5.1-18.0	1-500	0.8-2.8	6
	ASDE	12.94	121	1.61	0.5487	5.1-18.0	1-500	0.8-2.8	6
B.16	ASHS	9.96	100	1.62	0.5713	5.1-10.3	1-100	0.8-2.8	5
	ASDE	9.87	97	1.79	0.587	5.1-10.3	1-100	0.8-2.8	5
B.17	ASHS	13.12	118	2.10	0.4852	5.1-18.0	1-500	0.8-2.8	5
	ASDE	12.34	109	1.71	0.5001	5.1-18.0	1-500	0.8-2.8	5

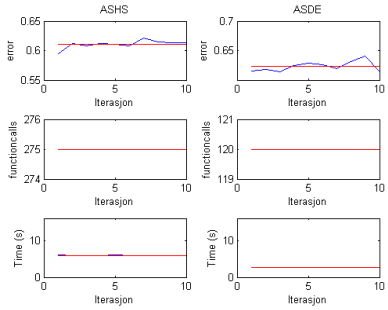

(a) Error, function calls and time used on estimation.

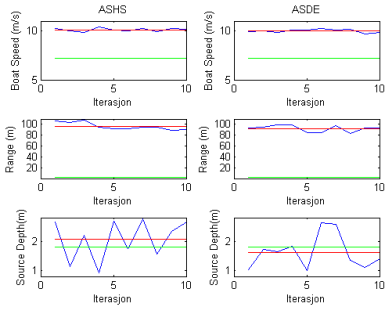

(b) Estimated parameters.

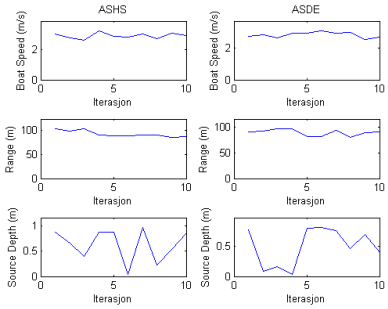

(c) Error of estimated parameters.

Figure B.14: ASHS and ASDE search of Småen, the blue line is the estimated value, the red is the mean value of the estimates and the green line is the real value. The search is done 10 times with the same parameters as for figure 4.16a, the d_s are unknown and with average search intervals, see table XXIV for the mean estimated parameters and the parameters used in the estimation.

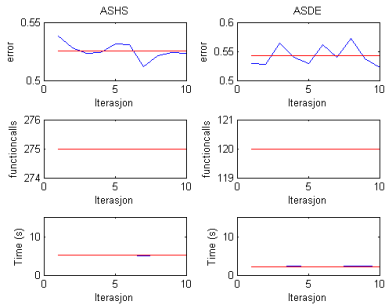

(a) Error, function calls and time used on estimation.

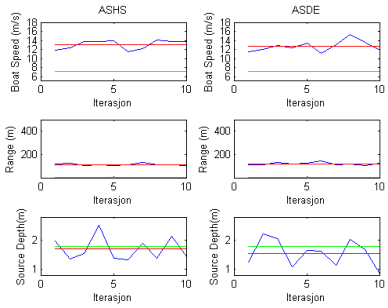

(b) Estimated parameters.

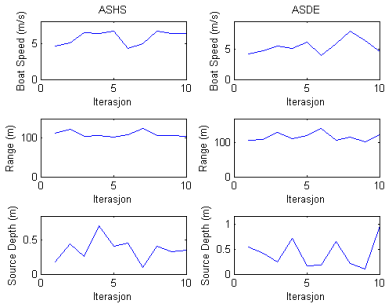

(c) Error of estimated parameters.

Figure B.15: ASHS and ASDE search of Småen, the blue line is the estimated value, the red is the mean value of the estimates and the green line is the real value. The search is done 10 times with the same parameters as for figure 4.16a, the d_s are unknown and with large search intervals, see table XXIV for the mean estimated parameters and the parameters used in the estimation.

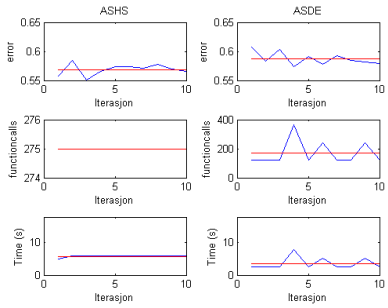

(a) Error, function calls and time used on estimation.

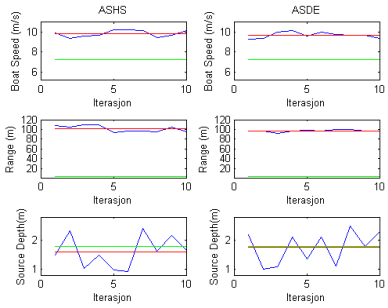

(b) Estimated parameters.

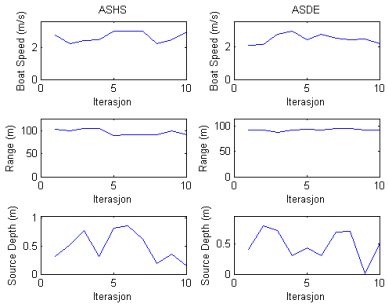

(c) Error of estimated parameters.

Figure B.16: ASHS and ASDE search of Jumbo, the blue line is the estimated value, the red is the mean value of the estimates and the green line is the real value. The search is done 10 times with the same parameters as for figure 4.16b, the d_s are unknown and with average search intervals, see table XXIV for the mean estimated parameters and the parameters used in the estimation.

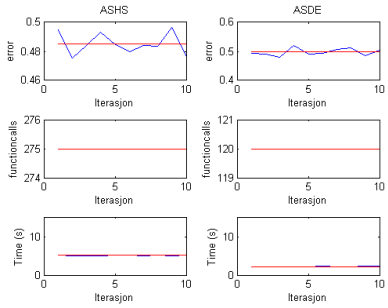

(a) Error, function calls and time used on estimation.

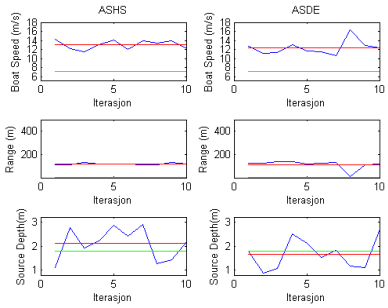

(b) Estimated parameters.

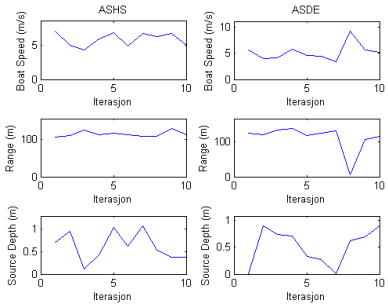

(c) Error of estimated parameters.

Figure B.17: ASHS and ASDE search of Jumbo, the blue line is the estimated value, the red is the mean value of the estimates and the green line is the real value. The search is done 10 times with the same parameters as for figure 4.16b, the d_s are unknown and with large search intervals, see table XXIV for the mean estimated parameters and the parameters used in the estimation.